

Peptidomimetic α -Acyloxymethylketone Warheads with Six-Membered Lactam P1 Glutamine Mimic: SARS-CoV-2 3CL Protease Inhibition, Coronavirus Antiviral Activity, and *in Vitro* Biological Stability

Bing Bai, Alexandr Belovodskiy, Mostofa Hena, Appan Srinivas Kandadai, Michael A. Joyce, Holly A. Saffran, Justin A. Shields, Muhammad Bashir Khan, Elena Arutyunova, Jimmy Lu, Sardeev K. Bajwa, Darren Hockman, Conrad Fischer, Tess Lamer, Wayne Vuong, Marco J. van Belkum, Zhengxian Gu, Fusen Lin, Yanhua Du, Jia Xu, Mohammad Rahim, Howard S. Young, John C. Vederas, D. Lorne Tyrrell, M. Joanne Lemieux, and James A. Nieman*



Cite This: <https://doi.org/10.1021/acs.jmedchem.1c00616>



Read Online

ACCESS |



Metrics & More

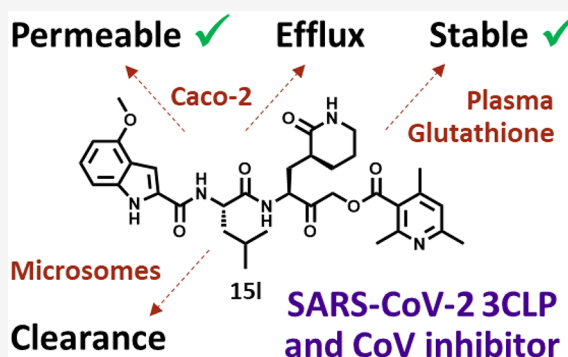


Article Recommendations



Supporting Information

ABSTRACT: Recurring coronavirus outbreaks, such as the current COVID-19 pandemic, establish a necessity to develop direct-acting antivirals that can be readily administered and are active against a broad spectrum of coronaviruses. Described in this Article are novel α -acyloxymethylketone warhead peptidomimetic compounds with a six-membered lactam glutamine mimic in P1. Compounds with potent SARS-CoV-2 3CL protease and *in vitro* viral replication inhibition were identified with low cytotoxicity and good plasma and glutathione stability. Compounds **15e**, **15h**, and **15l** displayed selectivity for SARS-CoV-2 3CL protease over CatB and CatS and superior *in vitro* SARS-CoV-2 antiviral replication inhibition compared with the reported peptidomimetic inhibitors with other warheads. The cocrystallization of **15l** with SARS-CoV-2 3CL protease confirmed the formation of a covalent adduct. α -Acyloxymethylketone compounds also exhibited antiviral activity against an alphacoronavirus and non-SARS betacoronavirus strains with similar potency and a better selectivity index than remdesivir. These findings demonstrate the potential of the substituted heteroaromatic and aliphatic α -acyloxymethylketone warheads as coronavirus inhibitors, and the described results provide a basis for further optimization.



INTRODUCTION

Viruses in Group IV of the Baltimore classification system have a positive-sense single-stranded RNA genome.¹ Members of Group IV are responsible for a range of diseases that cause mortality and morbidity in birds and mammals. Many Group IV viruses also infect humans, including rhinoviruses, noroviruses, and coronaviruses. Human rhinoviruses are responsible for up to 40% of the seasonal common cold,² and human noroviruses cause acute gastroenteritis, resulting in an estimated 50 000 deaths worldwide per year.³ The current global Coronavirus Disease 2019 (COVID-19) pandemic is caused by Severe Acute Respiratory Syndrome Coronavirus 2 (SARS-CoV-2), which is a member of the *Coronaviridae* family.⁴ Other coronaviruses are responsible for a portion of common seasonal colds as well as 2003 Severe Acute Respiratory Syndrome (SARS, caused by the SARS-CoV-1), and 2012 Middle East Respiratory Syndrome (MERS, caused by the MERS-CoV). Coronaviruses have four genera with two,

the alpha- and betacoronaviruses, descending from the bat viral gene pool, with SARS-CoV-1, MERS-CoV, and SARS-CoV-2 being betacoronaviruses.^{5–7}

Rhinoviruses, noroviruses, and coronaviruses share a similar protease critical for processing the viral polyprotein required for viral replication in the host cells.⁸ The peptide sequence cleaved by a protease is labeled as P3P2P1↓P1'P2'P3', where the amide bond cleavage occurs between P1 and P1', as indicated by the arrow, and the corresponding sites on the protease protein are referred to as S3S2S1S1'S2'S3'.^{8b} For rhinoviruses, noroviruses, and coronaviruses, this main

Special Issue: COVID-19

Received: April 4, 2021



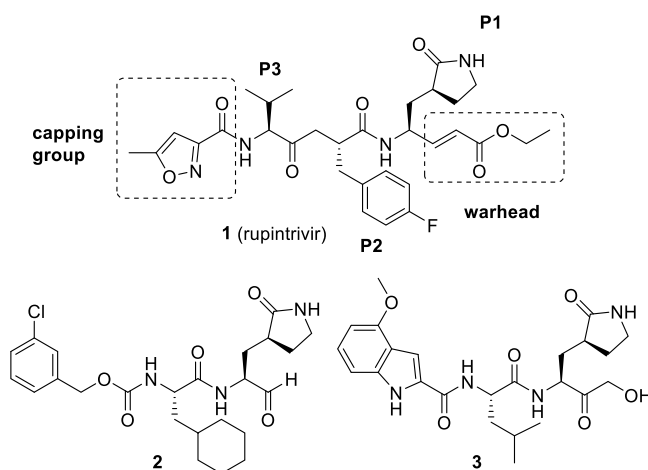


Figure 1. Published protease inhibitors for rhinovirus 3CP (**1**, rupintrivir), norovirus 3CLP **2**, and SARS 3CLP (**3**, PF-835231).

protease is a cysteine protease that primarily hydrolyzes proteins between a P1 glutamine and a small P1' amino acid, such as alanine or glycine.⁸ For rhinovirus, this protease is called 3C protease (3CP), whereas for norovirus and coronavirus, it is 3C-like protease (3CLP, 3CLP^{pro}, or M^{pro}). Beyond P1 and P1', significant differences in substrate specificity are observed. For example, Zhang and coworkers with a series of crystal structures observed significant shape and volume differences for S2 in different coronaviruses.^{8d}

Rhinovirus 3CP is the target of the clinically evaluated compound rupintrivir (**1**, Figure 1).⁹ During the rupintrivir drug discovery project at Agouron (Pfizer), a five-membered lactam at P1 was identified as a favorable glutamine replacement, where the peptidomimetic labels P1, P2, and P3 align with those of the substrates.² The five-membered lactam at P1 has been used in compounds directed against other Group IV viruses, besides rhinovirus 3CP, like norovirus 3CLP compound **2**¹⁰ and the published SARS-CoV-1 3CLP inhibitor **3** (Figure 1).¹¹ The α,β -unsaturated ester moiety, referred to as the warhead, in **1** reacts with the catalytic sulfur of the cysteine protease to form an irreversible, covalent bond. Compounds **2** and **3** have different warheads, an aldehyde and a carbonyl of an α -hydroxymethylketone, respectively, that form reversible, covalent adducts with the sulfur.^{10,11}

In 2017, the Li Ka Shing Applied Virology Institute (LKSAPI) began to explore direct acting antivirals to treat norovirus infections. Different viral targets were examined, including the polymerase¹² and peptidomimetic cysteine 3CLP inhibitors. Utilizing the literature at the time, various compounds were generated as part of the 3CLP portion of that program. What was not observed in the literature was that P2 cyclohexylalanine, such as in **2**, had cytotoxicity when combined with numerous different warhead types, potentially indicating significant cellular protease inhibition or metabolism of the cyclohexylalanine residue. Recently, others have also observed the cytotoxicity of cyclohexylalanine at P2.¹³

The outbreak of COVID-19 was first reported in December 2019 in Wuhan, China. To date, over 2.3 million people have died as a result of this ongoing pandemic.¹⁴ Although fatalities resulting from COVID-19 can impact any age group, the elderly, those with underlying health conditions, and individuals who have poor or nonexistent health care access are the most likely to perish due to this disease.¹⁴ Without intervention, tens of millions of people can be anticipated to

die as a result of COVID-19. Although vaccines were recently approved and are being administered as rapidly as possible, there will still be a need for therapeutics for future coronavirus variants and strains that evade the immune system as well as for those individuals who are immunocompromised. Currently, the only direct-acting antiviral that has been authorized for use is remdesivir, which was originally in clinical trials as an Ebola treatment.¹⁵ It is administered intravenously and has demonstrated only modest efficacy for moderate COVID-19.¹⁶ Novel therapeutics to treat coronavirus infections, especially ones with a different mechanism of action and that can be given orally, are needed not only now but also for potential future coronavirus outbreaks.¹⁷

Shortly after COVID-19 was declared a pandemic, a few noncytotoxic compounds from the legacy LKSAPI norovirus project were tested for their anti-SARS-CoV-2 3CLP activity. Compounds **4** and **5** (Figure 2) both had activity against 3CLP, with **5** demonstrating a submicromolar IC₅₀. Modest antiviral activity was also observed for **4** and **5** in a SARS-CoV-2 plaque reduction assay (PRA), which led us to start examining derivatives.

Despite the success of targeting metalloproteases as well as serine, threonine, and aspartyl proteases, to date, no cysteine

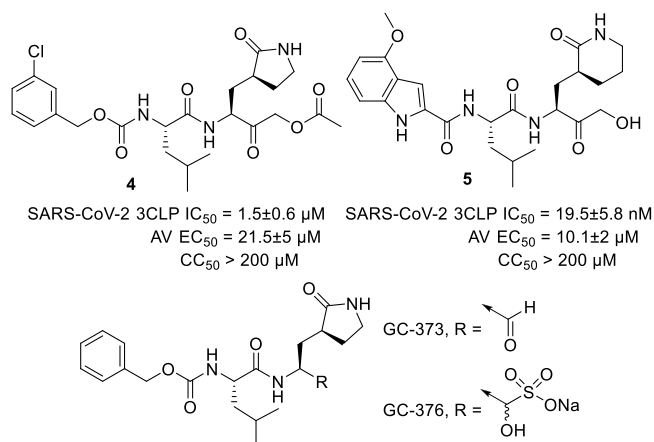


Figure 2. Exploratory noncytotoxic, norovirus project compounds **4** and **5** that were active when screened against SARS-CoV-2 3CLP and viral replication. Structure of GC-373 and its bisulfite adduct GC-376 that are reported SARS-CoV-2 3CLP inhibitors.

protease inhibitors have made it to market.¹⁸ Clinical failures of cysteine-protease-targeting drugs like odanacatib and rupintrivir demonstrate the challenges of drug discovery, and yet both demonstrated acceptable safety profiles to be evaluated in clinical trials.^{9,19} It is worth noting that both drugs are covalent inhibitors and did not appear to have significant toxicity on short-term dosing, the treatment time frame anticipated for an antiviral. The recent growth in successful covalent drugs, including targeting cysteine at or near the active site, has challenged the “all covalent inhibitors are toxic” dogma.^{20–22} Covalent inhibition of serine proteases has proven successful by utilizing the nucleophilic nature of the oxygen in the active site to block catalysis.²³ To successfully target the catalytic sulfur of cysteine in viral proteases, selectivity is required to avoid cytotoxicity as a result of inhibiting endogenous cysteine proteases. Excess reactivity will result in reaction with nucleophiles such as glutathione, which is present in the cytosol with a concentration range of 1–10 mM.²⁴ Optimal recognition elements for SARS-CoV-2 3CLP will help with selectivity and to reduce toxicity, but additional interaction and reactivity considerations will be critical to generate compounds with the antiviral potency, selectivity, and stability needed to become a safe drug.

Since the pandemic started, many diverse peptidomimetics have been examined for their ability to inhibit SARS CoV-2 3CLP. This rapid and impressive mobilization has included repurposing peptidomimetic drugs of other proteases and SARS-CoV-2 3CLP-targeted inhibitors, and most of these efforts have already been reviewed.²⁵ Many of the SARS-CoV-2 3CLP-targeted inhibitors build on results from the closely related SARS-CoV-1 3CLP investigation.²⁶ The SARS-CoV-2 3CLP-targeted inhibitors have almost exclusively utilized a five-membered lactam in P1, with a few recent six-membered P1 lactam examples (vide infra). The general warhead classes of peptidomimetics that have been studied for SARS-CoV-2 3CLP inhibition are enoate, aldehyde, ketoamide, and ketone.²⁵ Some noteworthy recent articles include utilizing an aldehyde warhead with an indole P3 capping group by Dai et al. and an aldehyde warhead with P2 hepatitis C virus (HCV) protease derivatives by Qiao et al., who observed *in vivo* efficacy in a mouse model.^{27,28} Other recent articles by Zhang et al. utilize a ketoamide^{8d,29} warhead with cyclopropylalanine P2 and a 2-pyridone capping group, and Jin et al. identified an enoate tetrapeptide inhibitor.³⁰ The most closely related recent article to the focus of the research we describe herein is from a group at Pfizer that developed peptidomimetic inhibitors, including **3**, against SARS-CoV-1¹¹ and more recently tested them against SARS-CoV-2 3CLP. That study will be discussed further as follows.

We decided to utilize a warhead that would generate an irreversible, covalent adduct. The α,β -unsaturated ester warhead of rupintrivir (**1**) reacts with the catalytic cysteine of rhinovirus 3CP in a Michael-like reaction to produce an irreversible adduct in the β -position.² We became interested in the work of Krantz and coworkers,³¹ in particular, their study with cathepsin B (CatB), although they also reported some structural work with papain, both of which are cysteine proteases, with a different consensus sequence and thus different P1, P2, and capping group preferences.³¹ Their CatB publications examined the leaving groups adjacent (α -position) to a ketone of an α -substituted methylketone.^{31ab} Krantz and coworkers observed that the pK_a of the leaving group correlated with the rate of irreversible, covalent inactivation.

The identity of the α -leaving group has to be chosen judiciously. Chloromethylketones, although useful synthetic intermediates, tend to be too reactive and are known to react with glutathione and to demonstrate cytotoxicity.³² A fluoromethylketone is more selective, but concerns with the metabolism generating the extremely toxic metabolite fluoroacetic acid creates challenges with pursuing a pharmaceutical agent with this warhead.³³ Other leaving groups like diphenylphosphinyl, tretronoyl, and peptidylesters were examined with another cysteine protease, interleukin-1 β converting enzyme, although no recent studies have been reported that study leaving group variations.^{34,35} Verhelst and coworkers examined a tetrapeptide with P1 glutamine, citrulline, and *N,N*-dimethylglutamine groups with a previously described 2,6-dimethylbenzoate α -cyloxymethylketone (AMK) as a molecular probe for SARS-CoV-2 3CLP inhibition. They reported a very low deactivation rate with these compounds and no antiviral results and concluded that the P1 residues were not optimal.³⁶ We decided to explore the α -acyloxy group that allows the pK_a to be adjusted to balance the rapid irreversible adduct formation and the excessive reactivity that sequester glutathione or cause cytotoxicity. The potential mechanisms of acyloxy displacement from the α -methyl of the AMK are shown in Figure 3, and the product formed after

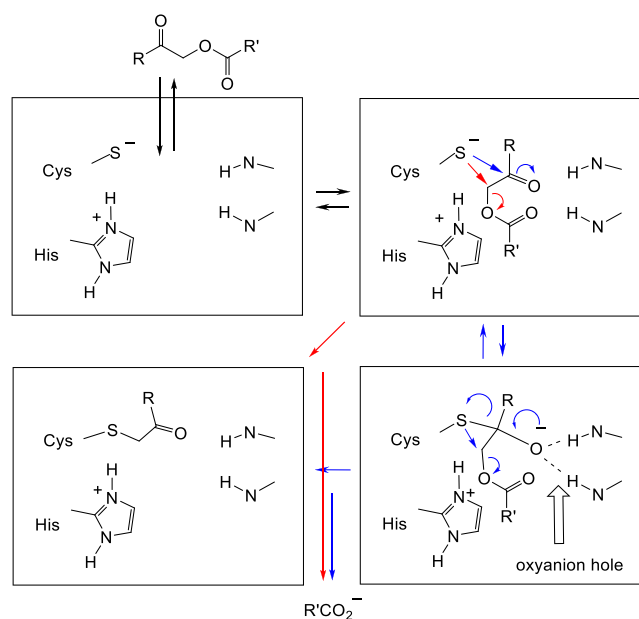
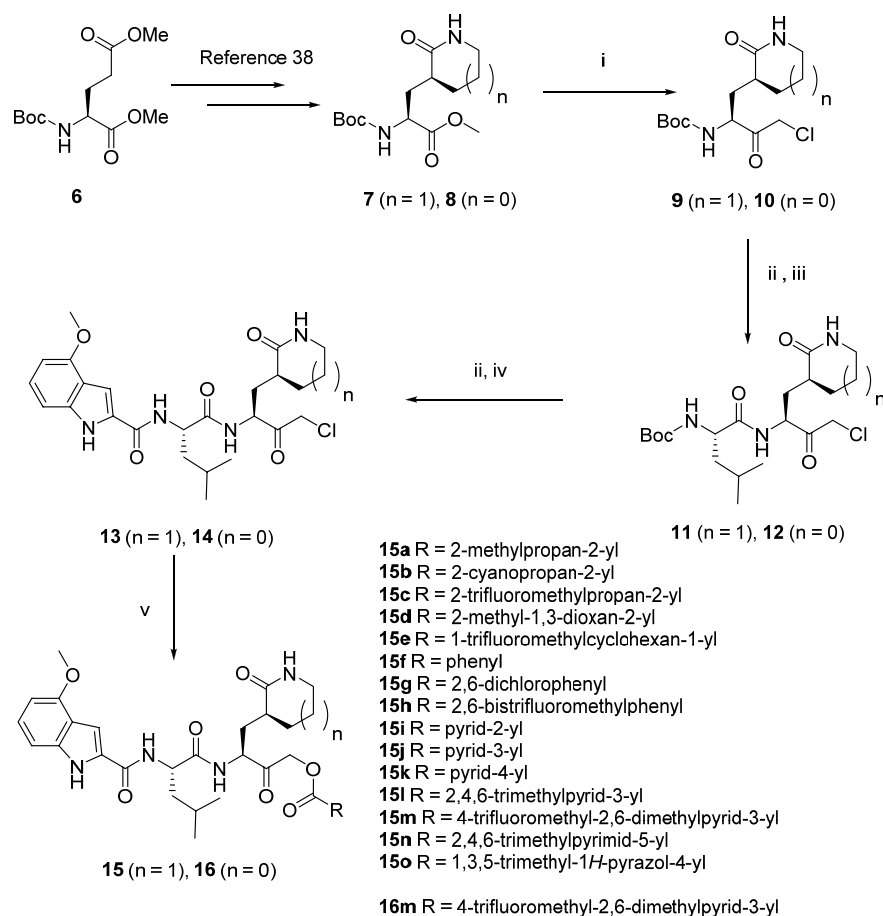


Figure 3. Potential mechanisms for the α -acyloxymethylketone covalent inhibition of cysteine proteases with the sulfur either directly displacing the acyloxy group (red arrows) or the sulfur attacking the carbon of the ketone (blue arrows) followed by sulfur migration. Both mechanisms produce the same product.

inactivation has been characterized by X-ray crystallographic and nuclear magnetic resonance (NMR) studies.³¹ Depending on the identity of R' in Figure 3, the ester could be rapidly hydrolyzed by esterases, preventing the irreversible, covalent adduct from forming because the resulting hydroxyl group is not displaced. Krantz and coworkers named these AMK warheads “quiescent affinity labels”, and their work focused exclusively on benzoate esters and a few aliphatic esters.^{31ab} That CatB study identified 2,6-bistrifluoromethyl and 2,6-dichloromethyl benzoates as potent, irreversible inactivators. To our knowledge there are no examples of heteroaromatic

Scheme 1. Synthesis of α -Acylloxymethylketone Compounds^a

^a(i) Sodium chloroacetate, Et₃N, *t*-BuMgCl, THF, 63% yield ($n = 1$), 60% yield ($n = 0$); (ii) HCl in dioxane, CHCl₃; (iii) Boc-L-leucine, HATU, NMM, DMF, 54% yield (two steps, $n = 1$), 47% yield (two steps, $n = 0$); (iv) 4-methoxyindole-CO₂H, HATU, NMM, DMF, 54% yield (two steps, $n = 1$), 42% (two steps, $n = 0$); (v) carboxylic acid, NaOt-Bu, NaI, DMF, 15–80% yield.

esters and only two examples, methoxyacetate by Krantz and peptidylesters by Dai et al., of electron-withdrawing-group-substituted aliphatic esters that improve the leaving group potential of the ester.^{31,35} Beside these two exceptions, most of the previously studied esters are very hydrophobic and planar (aromatic), which will cause challenges in optimizing the physicochemical properties, such as the aqueous solubility, to obtain good pharmacokinetic and drug-like properties. The heteroaromatic ester group we selected for examination allows the incorporation of additional polar surface area to potentially overcome this. The reduction of planarity, such as reducing the number of sp² carbons, can also improve the solubility and other properties, and this was our rationale for studying electron-withdrawing-group-substituted aliphatic esters. Because ester moieties can be rapidly cleaved by esterases *in vitro* and *in vivo*, the utilization of steric hindrance around the ester to slow hydrolysis is also an important consideration for good stability.

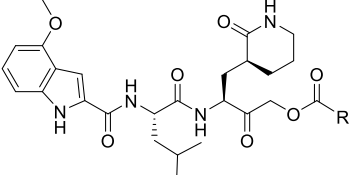
We decided to keep the 4-methoxyindole capping group and leucine in the P2 position of **5**. On the basis of literature searches at the time and reviews,³⁷ the six-membered glutamine mimic in P1 in **5** had not been examined against coronaviruses 3CLP, and so it was selected for P1, although it had been examined with retroviral aspartyl proteases (RVPs) and Enterovirus 71 3C proteases.^{2,38} With the remainder of the

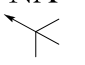
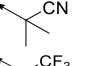

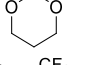
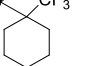
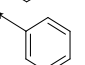
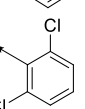
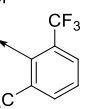
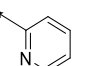
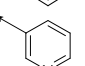
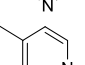
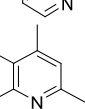
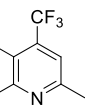
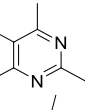
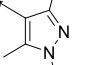
molecule held constant, a series of novel AMK-containing compounds were generated to assess their inhibition of both SARS-CoV-2 3CLP and SARS-CoV-2 replication, in addition to their cytotoxicity, stability (plasma and glutathione), cathepsin B and S selectivity, and ADME properties. After commencing our efforts, we were encouraged by the subsequent entry of PF-7304814, which is a phosphate prodrug for the hydroxymethylketone **3** reported in 2005,¹¹ into clinical trials as an IV treatment for COVID-19.^{39,40} Hoffman and coworkers reported AMK derivatives of **3** but focused on benzoates and other AMK groups previously reported by Krantz.^{11,39} The derivatives examined by Hoffman et al. did not include 2,6-bis(trifluoromethyl)benzoate, heterocyclic, or electron-withdrawing aliphatic AMK warheads or the P1 six-membered lactam described herein. We examined **3** in our SARS-CoV-2 3CLP FRET assay and found that it had an IC₅₀ value of 18.9 nM, which is similar to **5** (Figure 2). This reinforced our selection of **5** as a basis for studying AMK derivatives.

RESULTS

Chemistry. The synthetic routes utilized to generate the compounds are shown in Scheme 1 and were used with the six-membered lactam to generate **15a–15o** and with the five-membered P1 to generate **16m**.

Table 1. Compound Inhibition of SARS-CoV-2 3CLP and Viral Replication



CMPD	R	CLogP Chem Draw ^a	Carboxylic acid pK _a ^b	SARS CoV-2 3CLP IC ₅₀ (nM) ^c	PRA AV EC ₅₀ (μM) ^d	Vero E6 and A549 CC ₅₀ (μM)	SI
GC-376	NA	-	-	190 ± 40	0.9 ± 0.2	>100	>111
15a		1.85	5.03 ^e	64.1 ± 9.6	>10		
15b		1.39	2.4	21.9 ± 2.9	>10		
15c		2.28	3.2	20.0 ± 4	>5	>200	
15d		0.44	2.7	12.5 ± 4	>10		
15e		3.04	3.4	86.3 ± 0.1	0.6 ± 0.1	>200	>333
15f		1.82	4.204 ^e	63.5 ± 1	>10		
15g		2.94	1.26 ^e	6.4 ± 1.4	0.52 ± 0.2	>200	>385
15h		3.66	1.9	1.0 ± 0.17	0.16 ± 0.03	>200	>1,250
15i		0.91	0.99 ^e	125.5 ± 42	>10		
15j		0.48	2.00 ^e	4.0 ± 0.3	>10		
15k		0.48	1.77 ^e	32.9 ± 1.8	>10		
15l		2.38	1.7	19.0 ± 0.5	0.30 ± 0.02	>200	>667
15m		2.81	1.7	14.0 ± 1.7	0.47 ± 0.06	>200	>426
15n		2.20	2.0	22.1 ± 6	2.8 ± 1.1	>200	>71
15o		1.20	2.2	71.5 ± 6.5	>10		

^aChemDraw Prime version 16.0.1.4. ^bMeasured pK_a value unless otherwise indicated. ^cSee the Experimental Section for details, performed in triplicate with at least eight points in a single experiment. ^dSARS-CoV-2 (Vero E6 host cells) with compounds screened at 10 μM and the active ones tested at multiple concentrations to determine EC₅₀. ^eLiterature pK_a value for the corresponding carboxylic acid from ref 49.

The synthesis of intermediates 7 and 8 was accomplished starting from 6 following the procedure of Zhai et al.³⁸ The

conversion of the ester to the chloromethylketone utilized chemistry reported by Fukuyama and coworkers for their

synthesis of a key intermediate of FR901483.⁴¹ They utilized an *N*-Boc-protected phenylalanine generating an optically active intermediate that, like **7** and **8**, also had an epimerizable α -stereocenter. In previous literature, the five-membered lactam **10** was formed from **8** by saponification, diazomethane coupling, and HCl treatment or a one-step treatment of lithium diisopropylamine with chloriodomethane, the latter of which had poor reproducibility.^{11,39} In our hands, the one-step approach of Fukuyama more reliably produced **10** from **8** with a 60% yield and avoided the use of diazomethane. Using the same method with the six-membered lactam containing ester **7** generated the corresponding chloromethylketone **9** in 63% yield.

The chloromethylketones **9** and **10** were converted to **13** and **14**, respectively, following sequential deprotection and coupling protocols previously reported for **14**.^{11,39} Careful conversion of the chloromethylketone **13** to compounds **15a–15o** was required, as heating, extended reaction time, or excess base treatment produced a diastereomer, presumably at the stereogenic center next to the ketone. If the diastereomer formed, then it was readily observed by ¹H NMR and proved challenging to separate by silica gel chromatography. An example of this was compound **15o**, which was isolated with ~25% epimer. The exact reason for this higher diastereomer amount is unclear. It could be a result of the longer time to form the product during the overnight reaction, the susceptibility of the product to epimerization, or an issue with the diastereomeric integrity of the **13** batch used for this reaction. Compounds **15a–15n** had significantly less diastereomer based on ¹H and ¹⁹F NMR. (See the [Supporting Information](#).) For one of the most active compounds, ester **15m**, the five-membered lactam in P1 was produced. The reaction of 4-trifluoromethyl-2,6-dimethylnicotinic acid with **14** produced **16m**, which was isolated with high diastereomeric integrity based on ¹H and ¹⁹F NMR. (See the [Supporting Information](#).)

Biological Evaluation. Last year, a subset of authors of this manuscript reported the discovery that GC-373 and its bisulfite adduct GC-376 ([Figure 2](#)) display good anti-SARS-CoV-2 3CLP and antiviral activity (Vero E6 host).⁴² These 3CLP inhibitors contain a benzyl carbamate capping group, a P1 five-membered lactam, and an aldehyde warhead. For this LKSAPI study, we collaborated with those researchers and utilized the same SARS-CoV-2 3CLP biochemical and virological methods and protocols reported but focused on distinct molecules with AMK warheads, a 4-methoxyindole cap, and a six-membered P1 lactam.

The kinetics of protease inhibition by an AMK is complicated because the compounds can show differing degrees of both reversible and irreversible covalent inhibition.^{11,31,39} Even what appears to be reversible inhibition over longer timeframes produces a covalent adduct observed in cocrystal structures that is chemically irreversible.³⁹ Despite the complication of this bimodal nature, the ultimate goal is inhibition of coronavirus replication. To prevent viral replication *in vitro*, high levels of inhibition of the protease after only a short period are required to translate to robust antiviral activity, regardless of the degree of reversible and irreversible inhibition. Our plan was to identify the more active compounds based on the IC₅₀ values of the SARS-CoV-2 3CLP after a 30 min incubation period. We felt that this would provide insight into the team in an efficient manner. This approach is consistent with that recently reported by

Thorarensen and coworkers at Pfizer, who observed that an IC₅₀ determination after an incubation period was both insightful and an efficient method to assess trends for irreversible, covalent inhibitor programs.⁴³

Cytotoxicity plays a key role in interpreting antiviral activity, as viruses require healthy host cells to effectively replicate. One potential mechanism of cytotoxicity is the inhibition of cellular proteases that impact protein processing, and low or no cytotoxicity will suggest a degree of selectivity over other important proteases in a cellular assay. The selectivity index (SI) is a measure of cytotoxicity divided by antiviral activity (CC₅₀/EC₅₀). Active compounds that cause cytotoxicity, such as broad-spectrum cellular protease inhibition, will show SARS-CoV-2 antiviral activity and also reduced viability, resulting in a low SI (<10). Active compounds with low or no cytotoxicity will have antiviral activity and high viability, resulting in a high SI (>100). The results for benchmark GC-376 and AMK compounds **15a** to **15o** are shown in [Table 1](#). Compound GC-376, which is in clinical development as a feline infectious peritonitis (FIP) treatment and is now being considered as a COVID-19 treatment, has an IC₅₀ value of 190 nM for the SARS-CoV-2 3CLP.^{42,44} In comparison with a series of known protease inhibitors, GC-376 is one of the most potent inhibitors of SARS-CoV-2 3CLP.⁴⁵ All of the AMK compounds tested, **15a–15o**, had even lower IC₅₀ values than GC-376 ([Table 1](#)) against SARS-CoV-2 3CLP.

Compounds **15a–15e** are pivaloyl- and electron-withdrawing-group-substituted analogs designed to reduce the pK_a of the corresponding acid leaving group. The unsubstituted version, pivalate **15a**, showed an IC₅₀ of 64 nM. Krantz and coworkers, with different P1, P2, and capping groups targeting CatB, reported that the pivalate ester had a slow inactivation rate.^{31b} The related, but novel, warheads with a reduced pK_a of the corresponding acid are **15b–15e**, and each of these, with the exception of **15e**, were more active than **15a**; however, **15e** was still more active than GC-376. The benzoate derivative **15f**, also reported as a slow inactivator against CatB by Krantz,^{31b} had an essentially identical IC₅₀ to **15a** against SARS-CoV-2 3CLP. Substitutions on the 2,6-position to lower the pK_a of the corresponding acid resulted in reduced IC₅₀ values of 6.4 and 1.0 nM for the dichloro and bistrifluoromethyl compounds **15g** and **15h**, respectively. These were the best two benzoate ester inactivators reported by Krantz and coworkers for CatB.^{31b} These provided a comparison for our IC₅₀ value range for rapid inactivators. We then examined the use of pyridyl compounds, **15i**, **15j**, and **15k**, to reduce the pK_a of the corresponding acid leaving group compared with benzoate **15f**. Unexpectedly, we found, and subsequently confirmed on retest, that the nicotinate derivative **15j** was a potent inhibitor of SARS-CoV-2 3CLP, and its IC₅₀ value was in the range of the dichloro and bistrifluoromethyl derivatives, **15g** and **15h**. Substituted variations of **15j** were produced to improve better plasma stability (*vide infra*). Both **15l** and **15m** were less active against the SARS-CoV-2 3CLP than **15j**, but they were still about three times more active than the benzoate **15f**. Trimethyl-substituted pyrimidyl and pyrazole derivatives **15n** and **15o** were generated, but only the pyrimidyl derivative showed SARS-CoV-2 3CLP inhibition similar to **15l** and **15m**. The slopes of *k*_{obs} versus [I] graphs for five compounds, **15a**, **15e**, **15f**, **15h**, and **15l**, which represented a range of IC₅₀ and pK_a values, were determined ([Table S2](#)) and correlate well with the IC₅₀ values ([Chart S2](#)).

Compound GC-376 had an EC₅₀ value of 0.9 μM in the PRA with a cytotoxicity of >100 μM, resulting in an SI of >111 (Table 1 with SARS-CoV-2 and Vero E6 host cells). Compounds 15a–15o were initially screened at 10 μM, and any compound that did not reduce plaques by two-fold was assigned >10 μM. The compounds that significantly reduced the plaque numbers were examined in a concentration–response curve. Compound 15c had some reduction in plaques but did not meet the criteria to perform a concentration–response curve, and thus it was assigned >5 μM. The compounds that showed notable antiviral activity were 15e, 15g, 15h, 15l, 15m, and 15n. No toxicity was observed up to the highest concentration tested (200 μM) against the Vero E6 and A549 cell-lines, resulting in a high SI for all active compounds. Compounds 15e, 15g, 15h, 15l, and 15m were all more active than GC-376, and the most active of them, 15h and 15l, were established as some of the most potent SARS-CoV-2 antivirals reported.⁴⁶ Although numerous compounds had good SARS-CoV-2 3CLP IC₅₀ values, all of the compounds with a submicromolar EC₅₀ value in the PRA had a calculated LogP of 2.38 or greater. Compounds with a higher lipophilicity are anticipated to have higher permeability, which could explain why these compounds demonstrate better antiviral inhibition, despite similar protease IC₅₀ numbers.⁴⁷ Other factors, such as the stability in the presence of esterases, could also play a role during the PRA. Compounds with a lipophilicity of <3.0 are desirable,⁴⁸ and the calculated LogP values, with the exception of 15e, suggested that the compounds might have reasonable absorption, distribution, metabolism, and excretion (ADME) properties.

The compounds shown in Table 1 all had the six-membered lactam at P1. To evaluate the influence of the glutamine mimic at P1, the five-membered lactam version of 15m was synthesized, compound 16m (Figure 4). Compound 16m displayed an IC₅₀ against SARS-CoV-2 3CLP that was very close to that for 15m, and 16m showed a similar, or possibly slightly better, EC₅₀ in the PRA.

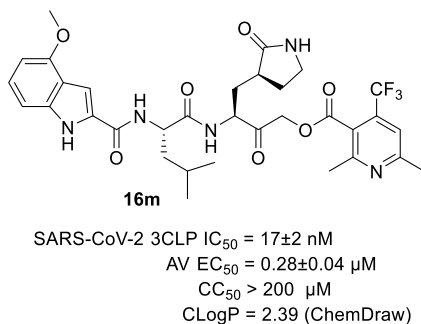


Figure 4. SARS-CoV-2 3CLP and antiviral results for five-membered lactam 16m.

To assess the spectrum of activity of these AMK warhead-containing peptidomimetics, we screened selected compounds against different coronaviruses in a cytopathic effect (CPE) assay. Table 2 shows the results against CoV-229E (alphacoronavirus) and CoV-OC43 (betacoronavirus) with remdesivir utilized as a positive control.

Our compounds had antiviral activity against the CoV-229E alphacoronavirus (MRC5 host cells) with EC₅₀ values ranging from 13 to 196 nM, with 15g, 15h, 15m, and 16m having better activity than remdesivir. The cytotoxicity observed

Table 2. Activity against Representative Alpha- and Betacoronaviruses

cmpd	229E CPE AV EC ₅₀ (μM) ^a	MRC5 CC ₅₀ (μM)	OC43 CPE AV EC ₅₀ (μM) ^a	Huh-7 CC ₅₀ (μM)
remdesivir	0.035	>100	0.020	10.37
15c	0.112	>100	0.195	94.61
15e	0.196	>100	0.395	>100
15g	0.021	>100	0.035	>100
15h	0.029	>100	0.047	94.61
15l	0.048	>100	0.054	>100
15m	0.030	>100	0.045	67.6
16m	0.013	>100	0.033	44.90

^aAverages of two experiments with Z' for 229E and OC43 consistently have been 0.79 ± 0.01 and 0.73 ± 0.01, respectively. 229E and OC43 CPE assays utilized MRC5 and Huh-7 host cells, respectively.

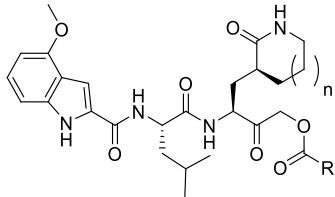
against the MRC5 cell line was >100 μM, which was the highest concentration tested, and was consistent with that observed in Table 1 against the Vero E6 and A549 cells. The SI was excellent for the compounds tested ranging from >510 to >7692 in the CoV-229E CPE assay.

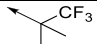
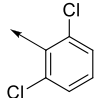
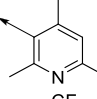
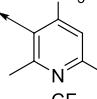
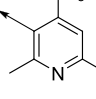
Our compounds also had excellent antiviral activity against the CoV-OC43 betacoronavirus (Huh-7 host cells). The EC₅₀ values were slightly higher than those against CoV-229E, although a different cell line was also utilized (Huh-7 vs MRC5) in addition to the different strain. Remdesivir was a more active inhibitor of CoV-OC43 replication than all of the compounds tested, although 15g, 15h, 15l, 15m, and 16m were only a few times less active. Remdesivir had a CC₅₀ value of 10.37 μM (SI = 518.5) against Huh-7 cells. Some of the compounds tested also had CC₅₀ values of <100 μM, although none were as low as the approved drug remdesivir. Compound 15m and 16m had the lowest CC₅₀ values, and yet their SIs were still 1502 and 1360, respectively, more than two times better than that of remdesivir.

ADME Evaluation. In a search of the literature for the stability and ADME properties assessment of peptidomimetic AMK groups, we found only one instance of a peptidyl ester, which was very unstable.³⁵ To determine if our AMK derivatives had acceptable properties for *in vivo* pharmacokinetic (PK) testing and efficacy studies, we assessed select compounds in an *in vitro* ADME panel (Table 3) and stability studies. These compounds are not predicted to be charged at physiological pH, so the LogD was anticipated to be similar to the LogP. The calculated LogP (ChemDraw) for the compounds was in an acceptable range; however, as can be seen in Table 3, the measured LogD (pH 7.4) was almost 2 units higher, all above 4, thus diminishing the probability that these compounds will have acceptable PK properties.⁴⁸

The aliphatic ester 15c was unstable in mouse plasma with a very short half life, suggesting that esterases present in the plasma are able to rapidly hydrolyze this hindered ester (Table 3). Compound 15g was also somewhat unstable in plasma, with a half life under 3 h. These two compounds also showed non-NADPH-dependent metabolism in the presence of microsomes and low recovery in the Caco-2 permeability assay (not shown). When examined in the presence of glutathione, both 15c and 15g underwent significant hydrolysis in the pH 7.4 buffer over 24 h at 37 °C (Table S1), with virtually no glutathione adduct formation.

Table 3. ADME Properties for Select Compounds



CMPD	R	n	Calculated LogP ^a	LogD (pH 7.4) ^{b,c}	Mouse Plasma Stability T _{1/2} (min) ^c	Mouse Microsomal Stability T _{1/2} (min) ^c	Mouse Hepatocyte Stability T _{1/2} (min) ^c	Caco-2 B to A Mean Papp (10 ⁻⁶ cm/s) [Efflux Ratio] ^c
15c		1	2.28	4.89	11.6	- ^d	- ^e	- ^f
15g		1	2.94	>5.07	169.7	- ^d	2.3	- ^f
15l		1	2.38	4.41	>289.1	1.1	2.7	21.8 [>45]
15m		1	2.81	4.11	>289.1	1.0	1.9	28.9 [1146]
16m		0	2.39	4.57	>289.1	1.1	1.9	24.3 [1751]

^aChemDraw Prime version 16.0.1.4. ^bShake flask method at 25 °C. ^cAverage of two different experiments with efflux ratio = B to A/A to B. ^dNon-NADPH-dependent elimination of compound observed with microsomes and compound in the absence of NADPH. ^eLoss of compound was observed in medium without cells. ^fInsufficient recovery due to nonspecific binding or instability in the matrix or other issues.

Compounds **15l**, **15m**, and **16m** were all stable in mouse plasma, were not metabolized independent of NADPH, and had good Caco-2 assay recovery (not shown). All three had LogD over 4, so it is understandable that they had short half lives in the presence of microsomes and hepatocytes. Their lack of NADPH-independent metabolism and their short $T_{1/2}$ in the presence of microsomes suggests that oxidative metabolism was the primary method of clearance of all three compounds. These three compounds also had good basolateral to apical (B to A) permeability of $>20 \times 10^{-6}$ cm/s in the Caco-2 assay; however, significant efflux was observed, suggesting that these structures, or portions of these structures, were recognized by an efflux transporter. Compounds **15l** and **15m** both showed $>80\%$ stability in the presence of 10 mM glutathione (pH 7.4) after 24 h at 37 °C, indicating reasonable stability to glutathione-mediated clearance and nominal nondiscriminant thiol reactivity (Table S1).

The hydrolysis of esters by esterases is influenced by a combination of steric and electronic factors.⁵⁰ Reducing the pK_a to more readily inhibit SARS-CoV-2 3CLP, such as in **15c** compared with **15a**, could also increase the rate of hydrolysis by an esterase in the plasma. To further understand the factors that might slow hydrolysis by esterases and not impact SARS-CoV-2 3CLP inhibition, we examined the rates of hydrolysis in human plasma (Table 4). The rapid hydrolysis of **15c** that

Table 4. Human Plasma Stability for Select Compounds

cmpd	human plasma stability	
	cmpd at 2 h (%) ^a	$T_{1/2}$ (min) ^b
15a	100	
15b	0	<15
15c	25	67
15e	97	
15f	67	209
15h	100	
15j	2	<15
15l	100	
15m	99	

^aAverage of two runs in relation to internal standard and hydrolyzed product **5**. ^bDetermined from four time points starting at 15 min and ending at 2 h.

occurred in mouse plasma also was observed in human plasma. In contrast, pivalate **15a** is very stable in human plasma, suggesting that the inductive influence of the CF₃ group in **15c** increased the hydrolysis rate despite the steric hindrance. Hydrolysis was extremely rapid for **15b**, further signifying that the electronic effects that reduced pK_a also contributed to the increased hydrolysis rate. Compound **15e** was significantly more stable than **15c** to esterases (Table 4) and was also more

Table 5. Human Cathepsin B and S Inhibition by Select Compounds

cmpd	inhibition			
	CatB % at 1 μ M	CatB IC ₅₀ (nM) ^a	CatS % at 1 μ M	CatS IC ₅₀ (nM) ^a
2	72.5 \pm 0.7		99.3 \pm 0.4	
5	26.5 \pm 1.7		60.8 \pm 4.4	
15e	38.6 \pm 0.5	2854 \pm 71	84.2 \pm 2.9	444 \pm 29
15f	16.2 \pm 7.4		41.0 \pm 7.4	
15h	91.3 \pm 1.6	464 \pm 24	96.8 \pm 0.2	116 \pm 11
15l	86.7 \pm 1.7	201 \pm 5	98.1 \pm 0.2	51.5 \pm 11.1
15m	95.0 \pm 1.2		98.4 \pm 0.4	

^aSee the [Experimental Section](#) for details. Performed in triplicate with six concentrations in a single experiment. Results were consistent with screening (triplicate) at 1 μ M.

resistant to hydrolysis in the presence of glutathione ([Table S1](#)). The CF₃ group in **15e** and **15c** is expected to have a similar electronic influence, and thus the increase in the steric bulk of the cyclohexyl group over the *gem*-dimethyl is likely responsible for the reduced hydrolysis rate observed for **15e**.

Benzoate esters are known to be substrates for esterases, as the results for **15f** confirm ([Table 4](#)).⁵⁰ The 2,6-bistrifluoromethyl substitution in **15h** increased the stability in human plasma compared with the benzoate. The nicotinate **15j** was more unstable in human plasma than benzoate **15h**. Substitution of two methyls or a methyl and a trifluoromethyl adjacent to the ester of **15j** generated compounds **15l** and **15m**, respectively, which both showed excellent stability in human plasma.

Literature 3CP and 3CLP peptidomimetics, such as **1**, **2**, and **3**, are reported to display low levels of inhibition of serine proteases and metalloproteases.^{2,10,39} Warheads, such as AMK and those in **1**, **2**, and **3**, are designed to react with the catalytic sulfur of the cysteine protease. In addition to assessing the glutathione reactivity ([Table S1](#)), it is prudent to also determine the selectivity over representative endogenous cysteine proteases, in particular, ones with similar specificities. For that reason, despite AMK compounds showing a high SI, we decided to measure their inhibition of two representative human cysteine proteases, cathepsin B (CatB) and cathepsin S (CatS). CatS has a similar consensus sequence to SARS-CoV-2 3CLP with specificities including a leucine in P2 and a glutamine in P1.⁵¹ Analogs of **1** and hydroxymethylketone-moiety-containing **3** are reported to demonstrate moderate CatB inhibition, although CatS inhibition was not reported.^{2,39} Krantz and coworkers examined their AMK analogs as CatB inhibitors, further justifying the selection of CatB to examine selectivity.^{31a,b} [Table 5](#) shows the results for select examples of our AMK compounds. For comparison we also screened an aldehyde warhead and norovirus 3CLP compound **2** (benchmark from the LKSAVI norovirus program) in addition to compound **5**, which is a P1 homologue of **3**.

Compounds were screened at 1 μ M with a 30 min incubation period to be consistent with SARS-CoV-2 3CLP inhibition results in [Table 1](#). CatS was inhibited by all of the compounds tested to a greater extent than CatB, suggesting a higher specificity of CatS for these P1 and P2 groups. Aldehyde **2** had the highest percent inhibition of CatS at 1 μ M. The inhibition of CatB with compound **5** was reasonably consistent with the IC₅₀ value of 1.3 μ M reported for analog **3**.³⁹ For the tested AMK compounds, the slow inactivator benzoate **15f** displayed the lowest percent inhibition of 16.2 and 41.0% for CatB and CatS, respectively. AMK compounds **15e**, **15h**, **15l**, and **15m** all displayed significant inhibition of CatB and CatS

at 1 μ M, with **15h**, **15l**, and **15m** displaying high levels of inhibition against both. The AMK compound **15l**, which had a pK_a of 1.7 for the corresponding acid leaving group, had the lowest IC₅₀ values against CatB and CatS. Compound **15h**, with a slightly higher measured pK_a of 1.9, displayed good 464- and 116-fold selectivity for SARS-CoV-2 3CLP over CatB and CatS, respectively. Compound **15e**, with a measured pK_a of 3.4 for the corresponding acid leaving group, had the highest IC₅₀ values of 2854 and 444 nM for CatB and CatS, respectively, compared with **15l** and **15h**. Compound **15e** displayed some selectivity, 33- and 5.6-fold, for SARS-CoV-2 3CLP over CatB and CatS, respectively.

Cocrystallization. To confirm that covalent inhibition was occurring, as depicted in [Figure 3](#), we performed cocrystallization experiments. Compound **15l**, which has an IC₅₀ value of 19 nM, was cocrystallized with SARS-CoV-2 3CLP. The cocrystal structure obtained had a resolution of 2.15 Å and is shown in [Figure 5](#) (PDB: 7MBI).

The SARS-CoV-2 3CLP–**15l** product crystallizes as a dimer, similar to other crystal structures of 3CLP. In the asymmetric

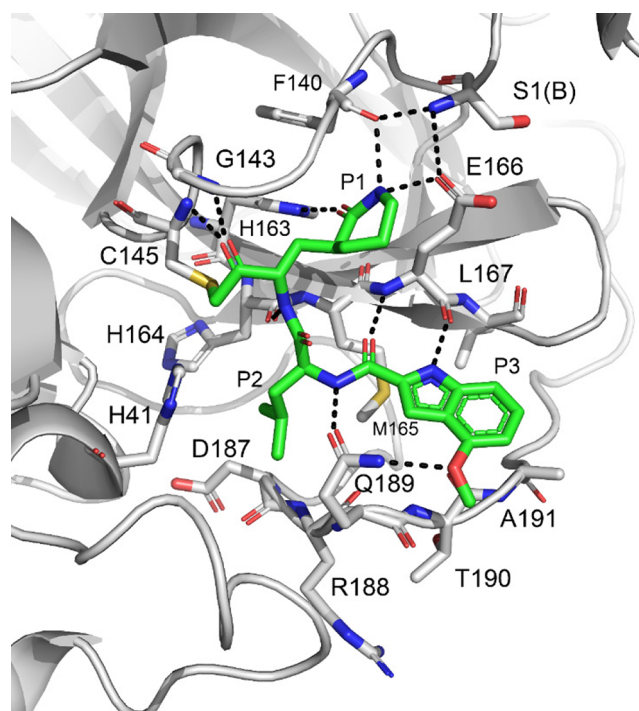


Figure 5. Cocrystal structure of chain C covalent adduct from **15l** reacting with SARS-CoV-2 3CLP (PDB: 7MBI).

unit, four protomers are found, and the 15l–3CLP structure with the active sites of each protomer produced the same adduct, although with slightly different orientations; see Figure S1 for an electron density map for all four protomers. Figure 5 shows the active site of one of the protomers (chain C). Overall, the orientation of this dipeptide in the P1 and P2 positions in the protease is similar to that of other inhibitors, yet the P3 position is extended compared with GC-376, for which P1 and P3 positions are stacked.^{39,42} Consistent with the mechanism in Figure 3, the 2,4,6-trimethylnicotinate group has been lost, and the sulfur of Cys145 has formed a covalent bond adjacent to the ketone with a C–S bond length of ~ 1.75 Å in each protomer. This type of covalent bond does not support reversibility, and because the sulfur is bonded to the α -carbon instead of the carbonyl carbon, this puts it out of alignment with that of the peptide substrate. This translocated attachment could impact the interactions of the peptidomimetic with the protein. In the protomer in Figure 5, the ketone oxygen is within hydrogen-bonding distance of Cys145 amide (3.1 Å N to O) and Gly143 (3.2 Å N to O) of the oxyanion hole. The six-membered lactam is picking up the same H-bonding interactions in S1 as the five-membered lactam for GC-376 and 3 structures.^{39,42} The lactam N is 2.7 Å to the carboxylic group of Glu166 and is 2.9 Å to the O of Phe140. The lactam carbonyl is oriented directly toward imidazole NH of His163 (2.8 Å). The isobutyl group of P2 is in a hydrophobic S2 pocket formed from Met49, Met165, and His41. For the capping group (P3), the indole N–H and the carbonyl of the amide make an H-bond donor and acceptor pair of bonds with Glu166, which is consistent with 3 and with indole GC-376 analogs.^{39,44} In this protomer (Figure 5), the O of the methoxy is within H-bonding distance with Gln189 (3.0 Å N to O). The ligand plot of chain C is shown in Figure S1. Despite the translocated attachment point, the H-bond interactions have been preserved in the active site of the different protomers.

DISCUSSION

Krantz and coworkers studied AMK warheads, primarily substituted benzoates, as part of a CatB study and found that 2,6-bistrifluoromethyl- and 2,6-dichloromethyl-substituted versions were rapid irreversible, covalent inhibitors.^{31b} They also found that benzoate and pivalate were slow inactivators. In our study, peptidomimetics 15g and 15h, designed for SARS-CoV-2 3CLP inhibition, resulted in single-digit nanomolar IC_{50} values. Compound 15h also showed good 464- and 116-fold selectivity for SARS-CoV-2 3CLP over CatB and CatS, respectively, and high plasma and glutathione stability, suggesting that 3CLP can be targeted selectively *in vivo* with AMK warheads. The slow inactivator esters, compounds 15a and 15f, both had an $IC_{50} \approx 65$ nM. This appeared consistent with Krantz's observations and provided a gauge for comparing our compounds. Other drug-like properties must be considered for *in vivo* testing; for example, we found that 2,6-dichloromethylbenzoate derivative 15g showed some instability in multiple *in vitro* stability assays. This instability is an important consideration, as 2,6-dichlorobenzoate AMK was examined in different efforts besides that of Krantz.^{34,39}

The electron-withdrawing-group-substituted aliphatic compounds 15b–15d (Table 1) had lower IC_{50} values against the SARS-CoV-2 3CLP than 15a and 15f, and one group, the 1-trifluoromethylcyclohex-1-yl of 15e, had a slightly higher value. For 15a to 15e, there is a general trend of the lower pK_a of the leaving acid having a lower IC_{50} value, but there are additional

factors involved, as it is not a direct correlation. For example, the higher IC_{50} of 15e compared with that of 15a, despite a 1.6 units lower pK_a of the corresponding carboxylic acid, might be a result of steric factors that cause an unfavorable interaction with 3CLP that impacts binding or hinders favorable alignment for inactivation. Compounds 15c and 15e also demonstrated good antiviral activity against both alpha- and betacoronavirus (Table 2), with their SI values being >253 . The instability of 15c was observed in plasma (mouse and human) and in the presence of both microsomes and hepatocytes. Compound 15e had significantly better human plasma stability, possibly indicating that a steric threshold was overcome to prevent rapid ester hydrolysis by esterases. In the presence of glutathione, compound 15e also showed excellent stability to both hydrolysis and reaction with glutathione (Table S1). Compound 15e had 33- and 5.6-fold selectivity for SARS-CoV-2 3CLP over CatB and CatS, respectively. The stability and antiviral activity of 15e is encouraging; however, the high lipophilicity contribution of the 1-trifluoromethylcyclohex-1-yl will need to be reduced, especially considering the significantly higher measured LogD observed for analogs in Table 3 compared with their calculated LogP.

For the picolinic, nicotinic, and isonicotinic esters (15i, 15j, and 15k, respectively, in Table 1) only the nicotinic ester showed a noteworthy 3CLP inhibition improvement compared with the benzoate 15f. Attempts to explain this observation by modeling failed to shed light on this inhibition preference, again confirming that other factors besides pK_a are important. Nicotinate 15j is very unstable in human plasma (Table 4), even more so than benzoate 15f. Substituting the nicotinate of 15j to improve the stability resulted in analogs 15l and 15m, both of which had a four times higher IC_{50} than 15j but still superior inhibition to benzoate 15f. Cocrystallizing 15l with SARS-CoV-2 3CLP showed that an irreversible, covalent product is ultimately formed. Compounds 15l and 15m and the five-membered lactam 16m had submicromolar EC_{50} values in the PRA and showed excellent antiviral inhibition of 229E and OC43 (an alpha- and betacoronavirus, respectively). The activities of these three protease inhibitors in the CPE assays were similar to those of remdesivir (Table 2). Compounds 15m and 16m showed some cytotoxicity in the Huh-7 cell line, but their SI values were still superior to that for remdesivir. The glutathione stability of 15l and 15m was good (Table S1), as was their plasma stability (human and mouse). The low metabolic stability in the presence of both hepatocytes and microsomes (Table 3) for 15l, 15m, and 16m is attributed to the high measured lipophilicity. Although the permeabilities for 15l, 15m, and 16m in the Caco-2 assay from the basolateral to the apical direction were good for all three compounds, efflux was an issue. Although the substituted nicotinic derivatives 15l and 15m have exciting activity with high SI values along with good plasma and glutathione stability, lipophilicity reduction will be required to improve the metabolic stability.⁴⁸ Modest selectivity was observed for 15l for SARS-CoV-2 3CLP over CatB and CatS. The lower pK_a for the corresponding acid leaving group of 15l might account for the lower selectivity, as it is anticipated to be more reactive. However, its higher IC_{50} value than that of 15h against SARS-CoV-2 3CLP, despite its lower pK_a , further reinforces that additional factors appear to be involved.

Based on the properties of 15l, trimethyl-substituted pyrimidyl and pyrazole were generated, derivatives 15n and 15o, respectively. Compound 15n, despite an IC_{50} value

against SARS-CoV-2 3CLP close to that of **15l** and **15m**, was less active in the PRA. The *N*-methyl-substituted pyrazole **15o** had a similar IC_{50} value to that of the reported slow inactivators, **15a** and **15f**. On the basis of the pK_a of the corresponding acid as a measure of the leaving group ability, compound **15o** with a 2 units lower pK_a should have improved inhibition compared with **15f**; however, it did not. The *N*-methyl potentially results in a less favorable interaction with the protein, negating any better leaving group ability.

Taken together the results for **15a** to **15o** show that refinement of the warhead leaving group has significant effects on the inhibition of SARS-CoV-2 3CLP. The lack of direct correlation of IC_{50} and pK_a of the corresponding leaving group indicates that other factors are important for determining the inhibition. Plotting k_{obs}/I versus pK_a for five compounds (**15a**, **15e**, **15f**, **15h**, and **15l**) also showed a trend toward lower pK_a leaving groups having a higher k_{obs}/I (Chart S1), and the poor correlation also reinforces that other factors appear to be involved besides pK_a . Plotting k_{obs}/I versus the IC_{50} value for the same compounds showed a good correlation of the lower IC_{50} value having a higher k_{obs}/I (Chart S2), which supports our decision to utilize IC_{50} as a gauge of activity against SARS-CoV-2 3CLP.

We found no reports of toxicity associated with the inhibition of other proteases for **2**, **3**, **3**'s prodrug PF-7304814, or FIP treatment GC-376, all of which have been examined *in vivo*. Compound **2** showed extremely potent CatS inhibition at 1 μ M. High SI (CC_{50}/EC_{50}) ratios were obtained for the AMK compounds, and considering other factors, such as the free fraction, their bimodal nature (varying degree of reversibility versus irreversibility), the acute treatment time frame, and enzyme turnover considerations, it is unclear what level of selectivity against related human cysteine proteases, such as CatS, is required for a drug discovery program. Potent inhibitors of CatS have been examined in clinical trials and "are, in general, well-tolerated by patients and healthy volunteers", although increased respiratory tract infection rates were observed in a small percentage of patients.⁵² Regardless, compound **15e**, **15h**, and **15l** showed selectivity over CatB and CatS.

Prior to commencing this work, we observed no publications examining six-membered P1 lactam as a coronavirus 3CLP inhibitor.^{45,46} Recently, variations with a different capping group and an aldehyde warhead were reported with modest SARS-CoV-1 and MERS 3CLP inhibition, and a patent application containing ketoamide warheads was published.^{53,54} The antiviral and protease results for **15m** and **16m** were similar, indicating that both lactams are reasonable glutamine mimics for SARS-CoV-2 3CLP. This observation is consistent with what was observed for rhinovirus 3CP peptidomimetics and with the recently published comparison with aldehyde warheads against MERS- and SARS-CoV-1 3CLP.^{2,53} This potentially represents a method to fine-tune the physicochemical properties of the peptidomimetic by selecting the five- or six-membered lactam in P1.

To achieve the ultimate goal of discovering a more readily administered 3CLP inhibitor to treat coronavirus infections, in particular, COVID-19 and its emerging variants, we will need to generate compounds with more favorable physicochemical properties. Accurately predicting the lipophilicity of the compounds before synthesis will be critical to generating compounds with improved properties. Upon the examination of some different lipophilicity prediction programs, it appears

that Marvin LogD might provide a closer approximation of experimental values for these peptidomimetics. With only a small number of compounds with measured LogD values, this preliminary observation will have to be confirmed. On the basis of the encouraging results for the select AMK groups previously described, the formation of analogs with a reduction in the lipophilicity will be required to improve the stability to oxidative metabolism.^{48b} Compounds with $CLogP > 2.38$ (Table 1) were able to demonstrate $EC_{50} < 1 \mu$ M in the PRA assay. This equates to a measured $LogD > 4$ (Table 3). In reducing the lipophilicity to decrease the rate of oxidative metabolism, additional alterations will be required to further improve or maintain the permeability or reduce the recognition by efflux transporters. It will also be important to lower the molecular mass or to reduce H-bond donors to improve the permeability and possibly lessen the efflux ratio.^{47,48d} Amide bond replacement (as was done toward rupintrivir),² warhead refinement, and indole replacement represent opportunities to achieve this. To assess the AMK group *in vivo*, molecules with improved physicochemical properties that maintain antiviral activity will have to be identified. It is our hope that this work enables that.

CONCLUSIONS

Although vaccines are now approved to prevent COVID-19, research into antivirals to treat immunocompromised individuals, variants, and future outbreaks is required. Coronaviruses, and related viruses, have a well-conserved cysteine protease that can be targeted to discover novel direct-acting antivirals. This study previously identified unexplored α -acyloxymethylketone derivatives that exhibited potent inhibition of SARS-CoV-2 3CLP and SARS-CoV-2 replication *in vitro*. Compounds **15l** and **15m** had activity similar to that of the top inhibitors reported in the literature and excellent plasma stability, despite containing an ester. High SIs were observed. Good glutathione stability and selectivity for SARS-CoV-2 3CLP over CatB and CatS signifies that discriminant reactivity can be obtained for these warheads. The cocrystallization of **15l** with the SARS-CoV-2 3CLP confirmed that a covalent adduct is formed. Compounds **15h**, **15l**, **15m**, and **16m** also had good antiviral potency against different coronavirus strains (CoV-229E and CoV-OC43). Assessing a six-membered lactam against its five-membered P1 counterpart (**15m** and **16m**) demonstrates that these two groups appear to be comparable in activity. Testing the more active compounds in an ADME panel indicated issues with oxidative metabolism and efflux transporter recognition, with the higher measured lipophilicity than predicted being the basis for the observed metabolic instability. These studies lay the foundation for optimizing these and related α -acyloxymethylketone warheads to obtain acceptable properties to facilitate more advanced studies.

EXPERIMENTAL SECTION

SARS-CoV-2 Protease FRET Assay and Determination of IC_{50} Values. Pure SARS-CoV-2 3CLP was obtained as previously described in detail, and the enzymatic activity was confirmed according to an established protocol; see ref 42. The FRET substrate was synthesized according to the methods previously described in ref 42. The IC_{50} values for each inhibitor tested were determined using methods described previously in ref 42 via a FRET-based kinetic assay with a 30 min inhibitor incubation period prior to the addition of the substrate. GraphPad Prism software (GraphPad 8.3.1) was used to determine the IC_{50} . Compounds were tested at eight different

concentrations (100 to 0.00001 μM). Triplicate experiments were performed for each data point, the appropriate Hill slopes were generated, and the value was presented as a mean \pm standard error.

SARS-CoV-2 Plaque Reduction Assay and Analysis. The EC_{50} and cytotoxicity determinations were carried out using the methods previously described in detail in ref 42 using SARS-CoV-2/Canada/VIDO 01/2020 and Vero E6 cells. Plaques were counted, and data were plotted as the percent inhibition versus \log_{10} [compound] using Prism (GraphPad). Assays were performed in duplicate with the EC_{50} determined with at least five different compound concentrations. EC_{50} values were calculated using a nonlinear regression analysis, and the value was presented as a mean \pm standard error.

OC43 and 229E High-Throughput CPE Assay. HCoV 229E and OC43 strains were acquired from the ATCC. MRC5 and Huh7 cells were obtained from the ATCC and AppTec, respectively. MRC5 cells were maintained in minimum essential medium (Sigma) supplemented with 10% fetal bovine serum (FBS) (ExCell), 1% L-glutamine (Gibco), 1% nonessential amino acid (NEAA) (Gibco), and 1% penicillin–streptomycin (HyClone). Minimum essential medium supplemented with 5% FBS, 1% L-glutamine, 1% NEAA, and 1% penicillin–streptomycin was used as the assay medium. Huh7 cells were maintained in the Dulbecco's modified Eagle's medium (Gibco) supplemented with 10% FBS, 1% L-glutamine, 1% NEAA, 1% sodium pyruvate (Gibco), and 1% penicillin–streptomycin.

Cells were seeded in 96-well plates (20 000 MRC5 and 8000 Huh7 cells per well) in 100 μL per well of assay medium at an appropriate density and cultured at 37 $^{\circ}\text{C}$ and 5% CO_2 overnight. Next day, the test compound was diluted with assay medium and then added to the cells, 50 μL per well. Then, 50 μL per well of assay-medium-diluted virus was added. The final volume of the cell culture was 200 μL per well. The final concentration of dimethyl sulfoxide (DMSO) in the cell culture was 0.5%. The resulting cell culture was incubated at 35 (229E) or 33 $^{\circ}\text{C}$ (OC43) and 5% CO_2 for an additional 3 (229E) or 7 (OC43) days until the virus infection in the virus control (cells infected with virus, without compound treatment) displayed a significant CPE. The CPE was measured by CellTiter Glo following the manufacturer's manual. The antiviral activity of compounds was calculated based on the protection against the virus-induced CPE at each concentration normalized by the virus control. The cytotoxicity of compounds was assessed under the same conditions, but without virus infection, in parallel. The cell viability was measured with CellTiter Glo following the manufacturer's manual. The antiviral activity and cytotoxicity of compounds were expressed as the % inhibition and the % viability, respectively, and were calculated with the following formulas

$$\text{inhibition (\%)} = \frac{(\text{raw data}_{\text{CPD}} - \text{average}_{\text{VC}})}{(\text{average}_{\text{CC}} - \text{average}_{\text{VC}})} * 100$$

$$\text{viability (\%)} = \frac{(\text{raw data}_{\text{CPD}} - \text{average}_{\text{MC}})}{(\text{average}_{\text{CC}} - \text{average}_{\text{MC}})} * 100$$

where raw data_{CPD} represents the values of the sample-treated wells, average_{VC} is the average value of the virus control, average_{CC} is average value of the cell control (cells without virus infection or compound treatment), and average_{MC} is the average value of the medium control (medium only) wells.

Compounds were tested at concentrations of 100, 20, 4, 0.8, 0.16, 0.032, 0.0064, and 0.00128 μM in duplicate. Remdesivir was used as a reference compound and was assayed starting from 1 and 100 μM for the EC_{50} and CC_{50} determinations, respectively. EC_{50} and CC_{50} values were calculated using the GraphPad Prism software with the equation "log(inhibitor) vs. response -- Variable slope (four parameters)". The historic Z' factor for the 229E and OC43 CPE assays is 0.79 \pm 0.01 and 0.73 \pm 0.01, respectively.

Crystallization of 3CLP with 15I. The purified SARS-CoV-2 3CLP was dialyzed against buffer containing 10 mM NaCl and 5 mM Tris HCl pH 8.0 overnight at 4 $^{\circ}\text{C}$. Protein was concentrated with a

Millipore centrifugal filter (10 kDa MW cutoff) to a concentration of 8 mg/mL. Protein was incubated with 5 mM excess of inhibitor at 4 $^{\circ}\text{C}$ for 1 h prior to crystallization. The SARS-CoV-2 3CL protein was subjected to the JCSG plus and PACT crystallization screen (Molecular Dimensions), with hits identified under several conditions for 15I. The best crystals were observed with sitting drop trays at room temperature at a ratio of 1:1 with mother liquor of 0.2 M sodium citrate tribasic dihydrate 0.1 M Bis-Tris propane pH 8.5 and 20% w/v PEG 3350. Prior to freezing, crystals were incubated with 22% glycerol as a cryoprotectant. Data collection took place at Stanford Synchrotron Radiation Lightsource (SSRL) (Menlo Park, CA) beamline 12-1 with Blu-Ice⁵⁵ using the Web-Ice interface⁵⁶ and at Canadian Light Source, Inc. (CLSI) beamline 08B1-1 using MxDC.

Diffraction Data Collection, Phase Determination, Model Building, and Refinement. X-ray diffraction data sets for SARS-CoV-2 3CLP and the inhibitor complex were collected at 100 K in a cold nitrogen stream using SSRL beamline 12-1 at a wavelength of 0.979460, equipped with an Eiger 16 M Pixel Array detector and using CLSI beamline 08B1-1 coupled to PILATUS 6M. Ten data sets were collected for the inhibitor, all of them were processed, and the best was selected based on data statistics. Energy-dispersive X-ray spectroscopy (XDS) and Scala were used for processing of the data sets. The diffraction data set of compound 15I with SARS-CoV-2 3CLP was processed at a resolution of 2.15 \AA in an orthorhombic space group $P2_12_12_1$ (Table S3). The structure was determined by molecular replacement, with the crystal structure of the free enzyme of the SARS-CoV-2 3CLP (PDB entry 6WTM)⁴² as a search model, using the Phaser program from Phenix, version v1.18.1-3855. The first unliganded SARS-CoV-2 3CLP structure was reported by Zhang and coworkers.²⁹ The ligand was fit using Coot manually for the inhibitor in the density of the precalculated map from the Phenix refinement. The refinement of the structure was performed with phenix.refine in Phenix software. The structure refinement yielded reasonable values of final R_{work} and R_{free} . The statistics of diffraction, data processing, and model refinement are given in the Supporting Information (Table S3). The model was inspected with Ramachandran plots, and all showed good stereochemistry. The final model was displayed using PyMOL molecular graphics software (version 2.0 Schrödinger).

Chemistry. All reagents and solvents were used as purchased from commercial sources. Moisture-sensitive reactions were carried out under a nitrogen atmosphere in oven-dried glassware. Reactions were stirred and were performed at ambient temperature, unless otherwise indicated. The reaction progress was monitored by TLC (precoated silica gel aluminum plates containing a fluorescent indicator (F-254)) with UV (254 nm) or staining (ninhydrin or phosphomolybdic acid) or alternatively by LC/MS. ¹H NMR, ¹³C NMR, and ¹⁹F NMR spectra were recorded at ambient temperature, unless otherwise indicated, with a Bruker Avance III 600 MHz NMR spectrometer equipped with a Bruker 5 mm PABBO probe. DEPTQ was run for ¹³C NMR. Chemical shifts are reported in ppm downfield from tetramethylsilane using residual solvent signals as the internal reference for ¹H NMR and ¹³C NMR. ¹⁹F NMR chemical shifts are reported relative to CFCl_3 . NMR spectra were processed utilizing an ACD/Spectrus processor (v2016.1.1, ACD/Laboratories) and Bruker TopSpin 4.0.6. Silica gel column purification was performed on a Biotage Isolera system with either Biotage or Silicycle cartridges. The LC/MS system used for monitoring the progress of the reactions and assessing the purity (absorbance at 254 nm) consisted of a Dionex ULTIMATE 3000 uHPLC module and a Thermo Scientific LTQ XL mass spectrometer with electrospray ionization and an Ion-Trap type of detector (alternating positive–negative mode). Separation was performed with a Thermo Scientific Accucore aQ C18 Polar End-capped LC column (100 mm \times 2.1 mm; particle size 2.6 μm , 80 \AA). The column was maintained at 30 $^{\circ}\text{C}$. Commercial high-performance liquid chromatography (HPLC)-grade methanol and domestic "Millipore (Milli-Q)" filtered water were used for chromatography and were modified by the addition of 0.1% (v/v) of formic acid. The eluent was delivered at a constant flow rate of 0.4 mL/min, and the column was equilibrated for 5 min with the corresponding eluent prior to injection of the sample (1 to 3 μL). The gradient (Eluent A)

was 45 to 95% methanol–water for 5.25 min followed by 5 min of isocratic 95% methanol–water. The purities of the final compounds were all >95%, as determined by UV (254 nm), and the corresponding m/z had the correct $M + H$ or $M - H$ signal with the appropriate isotope pattern. High-resolution mass spectrometry (HRMS) work was done on an LTQ Orbitrap XL (Thermo Scientific) apparatus operated in positive mode. Compound 2 was prepared as described in ref 10.

(3S)-3-[(N-[[[3-Chlorophenyl)methoxy]carbonyl]-L-leucyl]-amino]-2-oxo-4-[(3S)-2-oxopyrrolidin-3-yl]butyl Acetate (4). To a solution of 14 (1.02 g, 3.35 mmol) in *N,N*-dimethylformamide (DMF) (8 mL) was added NaI (494 mg, 3.30 mmol) and potassium acetate (647 mg, 6.60 mmol), and the solution was allowed to sit overnight. Saturated aqueous NH_4Cl solution was then added, and the mixture was extracted with EtOAc (3 × 40 mL). The combined organic layer was washed with a saturated aqueous NaHCO_3 solution and brine, dried over Na_2SO_4 , filtered, and concentrated under reduced pressure. The product was purified by column chromatography on silica gel with a gradient of 1–4% MeOH in dichloromethane (DCM), which generated (3S)-3-[(*tert*-butoxycarbonyl)-amino]-2-oxo-4-[(3S)-2-oxopyrrolidin-3-yl]butyl acetate (900 mg, 83% yield) as a light yellow foam. ^1H NMR (600 MHz, CDCl_3) δ 6.35 (br d, $J = 6.3$ Hz, 1H), 5.60 (br s, 1H), 4.97 (d, $J = 17.1$ Hz, 1H), 4.86 (d, $J = 17.1$ Hz, 1H), 4.40–4.32 (m, 1H), 3.43–3.34 (m, 2H), 2.53–2.41 (m, 2H), 2.18 (s, 3H), 2.13–2.06 (m, 1H), 1.95–1.84 (m, 2H), 1.47 (s, 9H).

To a solution of (3S)-3-[(*tert*-butoxycarbonyl)amino]-2-oxo-4-[(3S)-2-oxopyrrolidin-3-yl]butyl acetate (251 mg, 0.764 mmol) in DCM (3 mL) cooled in an ice bath was added trifluoroacetic acid (TFA) (1.5 mL). After 5 min, the ice bath was removed. After 1 h, the solvent was removed under reduced pressure. The residue was coevaporated with DCM/ether (1:1, 2 × 20 mL) and dried under vacuum. To the resulting residue was added *N*-[[[3-chlorophenyl)methoxy]carbonyl]-L-leucine (251 mg, 0.837 mmol) (prepared using the procedure in ref 10) and anhydrous DCM (10 mL). The resulting solution was cooled in an ice bath; then, HATU (433 mg, 1.14 mmol) followed by triethylamine (Et_3N) (0.250 mL, 1.83 mmol) was added. After 1 h, to the mixture was added an ice/saturated aqueous NaHCO_3 mixture (1:1, 10 mL). The two layers were separated, and the aqueous layer was extracted with DCM (2 × 30 mL), dried over Na_2SO_4 , filtered, and concentrated under reduced pressure. The product was purified by column chromatography on silica gel with a gradient of 1–3% MeOH in CHCl_3 , which generated 4 (170 mg, 44% yield) as a white solid. $R_f = 0.24$ (5% MeOH in DCM). ^1H NMR (600 MHz, $\text{DMSO}-d_6$, 334 K, D_2O exchange) δ 7.40–7.32 (m, 3H), 7.31–7.27 (m, 1H), 5.08–5.00 (m, 2H), 4.84–4.74 (m, 2H), 4.44–4.38 (m, 1H), 4.08–4.02 (m, 1H), 3.18–3.11 (m, 1H), 3.10–3.03 (m, 1H), 2.31–2.22 (m, 1H), 2.14–2.07 (m, 1H), 2.07 (s, 3H), 2.01–1.93 (m, 1H), 1.70–1.57 (m, 3H), 1.55–1.43 (m, 2H), 0.90 (d, $J = 6.6$ Hz, 1H), 0.87 (d, $J = 6.6$ Hz, 1H). LC/MS: 5.24 min retention time, 98.2% pure. ESI-MS: 510 $[\text{M} + \text{H}]^+$. HRMS (ESI+) calcd for $\text{C}_{24}\text{H}_{32}\text{ClN}_3\text{O}_7 + \text{H}$ 510.2007, found 510.2023.

N-[(2S)-1-[(2S)-4-Hydroxy-3-oxo-1-[(3S)-2-oxopiperidin-3-yl]butan-2-yl]amino]-4-methyl-1-oxopentan-2-yl]-4-methoxy-1H-indole-2-carboxamide (5). To oxo(phenyl)acetic acid (178 mg, 1.19 mmol) in anhydrous DMF (5 mL) was added sodium *tert*-butoxide (57.1 mg, 0.594 mmol). After 30 min, 13 (100 mg, 0.198 mmol) and NaI (59.4 mg, 0.396 mmol) were added. After 24 h, saturated brine (10 mL) was added, and the mixture was extracted with CHCl_3 (3 × 10 mL). The combined organic layer was washed with saturated brine (1 × 10 mL), dried over anhydrous Na_2SO_4 , filtered, and concentrated under reduced pressure. The crude was dissolved in CHCl_3 (10 mL) and loaded on silica gel column, and the product was purified by silica gel chromatography with a gradient of 0–6% MeOH in CHCl_3 , which afforded (3S)-3-[[*N*-(4-methoxy-1H-indole-2-carbonyl)-L-leucyl]amino]-2-oxo-4-[(3S)-2-oxopiperidin-3-yl]butyloxy(phenyl)acetate (62.6 mg, 51% yield) as an off-white solid. ^1H NMR (600 MHz, $\text{DMSO}-d_6$) δ 11.58 (d, $J = 2.1$ Hz, 1H), 8.67 (d, $J = 8.1$ Hz, 1H), 8.48 (d, $J = 7.6$ Hz, 1H), 8.11 (dd, $J = 1.0, 7.1$ Hz, 1H), 7.86–7.79 (m, 1H), 7.67 (t, $J = 7.8$ Hz, 2H), 7.47 (br s, 1H),

7.38 (d, $J = 1.7$ Hz, 1H), 7.11 (t, $J = 8.1$ Hz, 1H), 7.02 (d, $J = 8.2$ Hz, 2H), 6.51 (d, $J = 7.7$ Hz, 1H), 5.31 (d, $J = 17$ Hz, 1H), 5.25 (d, $J = 17$ Hz, 1H), 4.61–4.54 (m, 1H), 4.52–4.41 (m, 1H), 3.89 (s, 3H), 3.15–3.04 (m, 2H), 2.35–2.14 (m, 2H), 1.92–1.81 (m, 1H), 1.79–1.65 (m, 4H), 1.65–1.48 (m, 2H), 1.46–1.30 (m, 1H), 0.96 (d, $J = 6.3$ Hz, 3H), 0.91 (d, $J = 6.3$ Hz, 3H). ^{13}C NMR (151 MHz, $\text{DMSO}-d_6$) δ 209.7, 172.7, 172.7, 161.0, 153.6, 137.8, 129.9, 124.4, 118.1, 105.4, 101.1, 99.2, 65.5, 55.1, 52.7, 51.5, 41.2, 40.2, 37.0, 31.4, 25.5, 24.4, 23.0, 21.4, 21.1. LC/MS: 6.21 min retention time, 96.3% pure. ESI-MS: 619 $[\text{M} + \text{H}]^+$.

To a solution of (3S)-3-[[*N*-(4-methoxy-1H-indole-2-carbonyl)-L-leucyl]amino]-2-oxo-4-[(3S)-2-oxopiperidin-3-yl]butyloxy(phenyl)acetate (42.6 mg, 0.069 mmol) in THF/MeOH (1:1, 10 mL) was added CsF (1.05 mg, 0.0069 mmol), and the solution was allowed to sit overnight. Saturated brine solution (10 mL) was then added, and the mixture was extracted with CHCl_3 (3 × 10 mL). The combined organic layer was washed with saturated brine (1 × 10 mL), dried over anhydrous Na_2SO_4 , filtered, and concentrated under reduced pressure. The crude was dissolved in CHCl_3 (5 mL) and loaded on a silica gel column, and the product was purified by silica gel chromatography with a gradient of 0 to 2% MeOH in CHCl_3 , which afforded 5 (18.9 mg, 56% yield) as an off-white solid. $R_f = 0.18$ (5% MeOH in DCM). ^1H NMR (600 MHz, $\text{DMSO}-d_6$) δ 11.56 (br s, 1H), 8.46 (d, $J = 7.9$ Hz, 1H), 8.40 (d, $J = 7.6$ Hz, 1H), 7.43 (br s, 1H), 7.36 (br s, 1H), 7.10 (br t, $J = 7.7$ Hz, 1H), 7.01 (br d, $J = 7.9$ Hz, 1H), 6.51 (br d, $J = 7.5$ Hz, 1H), 5.04 (br t, $J = 5.6$ Hz, 1H), 4.55–4.44 (m, 2H), 4.26 (dd, $J = 6.0, 18.5$ Hz, 1H), 4.15 (dd, $J = 6.0, 18.5$ Hz, 1H), 3.89 (s, 3H), 3.15–3.02 (m, 2H), 2.27–2.08 (m, 2H), 1.91–1.80 (m, 1H), 1.78–1.63 (m, 4H), 1.60–1.45 (m, 2H), 1.40–1.22 (m, 1H), 0.95 (br d, $J = 6.0$ Hz, 3H), 0.90 (br d, $J = 6.0$ Hz, 3H). LC/MS: 4.23 min retention time, 98.7% pure. ESI-MS: 487 $[\text{M} + \text{H}]^+$. HRMS (ESI+) calcd for $\text{C}_{25}\text{H}_{34}\text{N}_4\text{O}_6 + \text{H}$ 487.2557, found 487.2565.

tert-Butyl {(2S)-4-Chloro-3-oxo-1-[(3S)-2-oxopiperidin-3-yl]butan-2-yl}carbamate (9). To a solution of 7 (7.00 g, 23.3 mmol) (prepared using methods in ref 38), sodium chloroacetate (8.96 g, 76.9 mmol), and Et_3N (10.7 mL, 76.9 mmol) in anhydrous tetrahydrofuran (THF) (200 mL) cooled in an ice bath was added a solution of 2.0 M *tert*-butylmagnesium chloride solution in THF (116.5 mL, 233 mmol) via a dropping funnel over 1.5 h.⁴¹ After 30 min, the ice bath was removed. After 18 h at room temperature, ice was then added, followed by the addition of a precooled 4 N HCl aqueous solution to carefully adjust the pH to 7. The two layers were separated, and the aqueous layer was extracted with EtOAc (3 × 150 mL). The combined organic phase was washed with brine (100 mL), dried over Na_2SO_4 , filtered, and concentrated under reduced pressure. The product was purified by column chromatography on silica gel with a gradient of 50–100% EtOAc in hexanes, which generated 9 (4.7 g, 63% yield) as a white foam. $R_f = 0.44$ (5% MeOH in EtOAc) was a single spot when visualized with 10% phosphomolybdic acid in ethanol. ^1H NMR (600 MHz, $\text{DMSO}-d_6$) δ 7.51 (d, $J = 7.5$ Hz, 1H), 7.49 (br s, 1H), 4.65–4.56 (m, 2H), 4.23–4.16 (m, 1H), 3.15–3.07 (m, 2H), 2.18–2.10 (m, 1H), 2.05–2.00 (m, 1H), 1.92–1.86 (m, 1H), 1.80–1.73 (m, 1H), 1.71–1.64 (m, 1H), 1.61–1.52 (m, 1H), 1.40–1.37 (m, 9H), 1.36–1.34 (m, 1H).

tert-Butyl {(2S)-4-Chloro-3-oxo-1-[(3S)-2-oxopyrrolidin-3-yl]butan-2-yl}carbamate (10). To a solution of 8 (8.5 g, 29.7 mmol) (prepared using the method in ref 38), sodium chloroacetate (11.4 g, 98.0 mmol), and Et_3N (13.6 mL, 98.0 mmol) in anhydrous THF (250 mL) cooled in an ice bath was added a solution of 2.0 M *tert*-butylmagnesium chloride solution in THF (148.5 mL, 297 mmol) via a dropping funnel over 1.5 h.⁴¹ After 30 min, the ice bath was removed. After 18 h at room temperature, ice was then added, followed by a precooled 4 N HCl aqueous solution to carefully adjust the pH to 7. The two layers were separated, and the aqueous layer was extracted with EtOAc (3 × 150 mL). The combined organic phase was washed with brine (100 mL), dried over Na_2SO_4 , filtered, and concentrated under reduced pressure. The product was purified by column chromatography on silica gel with a gradient of 0 to 1% MeOH in EtOAc, which generated 10 (5.45 g, 60% yield) as a white

foam. The product was consistent with that produced by established methods.^{11,39}

*N*²-(*tert*-Butoxycarbonyl)-*N*-{[(2*S*)-4-chloro-3-oxo-1-[(3*S*)-2-oxopiperidin-3-yl]butan-2-yl]-*L*-leucinamide (11). A solution of 9 (3.70 g, 11.6 mmol) in CHCl₃ (50 mL) was cooled using an ice–water bath; then, 4 M HCl in 1,4-dioxane (14.5 mL) was added. After 30 min, the ice bath was removed, the mixture was warmed to room temperature, and the solution was allowed to sit overnight. An off-white precipitate was then formed, and the mixture was concentrated under reduced pressure (30 °C water bath temperature), coevaporated with acetonitrile (3 × 20 mL) and DCM (1 × 20 mL), and dried for an additional 1 h under reduced pressure to afford (3*S*)-3-[(2*S*)-2-amino-4-chloro-3-oxobutyl]piperidin-2-one hydrochloride salt (2.96 g) as a cream color solid. This material was used without further purification in the next step. ¹H NMR (600 MHz, DMSO-*d*₆) δ 8.55 (br s, 3H), 7.80 (br s, 1H), 4.90 (d, *J* = 16.9 Hz, 1H), 4.74 (d, *J* = 16.9 Hz, 1H), 4.37–4.29 (m, 1H), 3.17–3.07 (m, 2H), 2.47–2.38 (m, 1H), 2.12–2.05 (m, 1H), 2.01–1.88 (m, 2H), 1.83–1.74 (m, 1H), 1.68–1.55 (m, 2H), 1.50–1.36 (m, 1H).

To a solution of (3*S*)-3-[(2*S*)-2-amino-4-chloro-3-oxobutyl]piperidin-2-one hydrochloride salt (2.96 g, maximum of 11.6 mmol) and *N*-(*tert*-butylcarbonyl)-*L*-leucine (5) (2.95 g, 12.8 mmol) in anhydrous DMF (50 mL) cooled in an ice bath was added HATU (4.85 g, 12.8 mmol). Then, *N*-methylmorpholine (NMM) (3.83 mL, 34.8 mmol) was added dropwise. After 45 min, an ice/saturated aqueous NaHCO₃ mixture (1:1, 200 mL) was added, and the resulting mixture was extracted with ethyl acetate (3 × 250 mL). The combined organic layer was washed with saturated brine solution (1 × 250 mL), dried over anhydrous Na₂SO₄, filtered, and concentrated under reduced pressure. The resulting residue was dissolved in CHCl₃ (20 mL), and the product was purified by silica gel chromatography with a gradient of 0–4% MeOH in CHCl₃, which generated 11 (2.70 g, 54% yield) as a white foamy solid. *R*_f = 0.50 (5% MeOH in EtOAc) was a single spot when visualized with 10% phosphomolybdic acid in ethanol. ¹H NMR (600 MHz, DMSO-*d*₆) δ 8.45 (d, *J* = 7.9 Hz, 1H), 7.46 (br s, 1H), 7.04 (br d, *J* = 7.2 Hz, 1H), 4.61 (d, *J* = 16.7 Hz, 1H), 4.54 (d, *J* = 16.7 Hz, 1H), 4.50–4.39 (m, 1H), 3.93–3.86 (m, 1H), 3.14–3.06 (m, 2H), 2.22–2.09 (m, 2H), 1.90–1.83 (m, 1H), 1.80–1.57 (m, 4H), 1.57–1.48 (m, 1H), 1.48–1.41 (m, 1H), 1.38 (s, 9H), 1.34–1.23 (m, 1H), 0.89 (d, *J* = 6.6 Hz, 3H), 0.85 (d, *J* = 6.6 Hz, 3H).

*N*²-(*tert*-Butoxycarbonyl)-*N*-{[(2*S*)-4-chloro-3-oxo-1-[(3*S*)-2-oxopyrrolidin-3-yl]butan-2-yl]-*L*-leucinamide (12). This material was prepared using procedures in refs 11 and 39.

N-[(2*S*)-1-[(2*S*)-4-chloro-3-oxo-1-[(3*S*)-2-oxopiperidin-3-yl]butan-2-yl]amino)-4-methyl-1-oxopentan-2-yl]-4-methoxy-1*H*-indole-2-carboxamide (13). A solution of 11 (2.70 g, 6.25 mmol) in CHCl₃ (25 mL) was cooled using an ice–water bath; then, 4 M HCl in 1,4-dioxane (10 mL) was added. After 30 min, the ice bath was removed, and the solution was allowed to sit overnight. A gummy precipitate was then formed. The mixture was then concentrated under reduced pressure (bath temperature at 35 °C), coevaporated with acetonitrile (3 × 20 mL) and DCM (1 × 20 mL), and dried under reduced pressure for 1 h to afford *N*-{[(2*S*)-4-chloro-3-oxo-1-[(3*S*)-2-oxopiperidin-3-yl]butan-2-yl]-*L*-leucinamide hydrochloride salt (2.30 g) as an off-white color solid. This material was used without further purification in the next step. ¹H NMR (600 MHz, DMSO-*d*₆) δ 9.13 (d, *J* = 7.5 Hz, 1H), 8.33 (br d, *J* = 3.8 Hz, 3H), 7.53 (br s, 1H), 4.68 (s, 2H), 4.56 (ddd, *J* = 4.0, 7.3, 11.1 Hz, 1H), 3.86–3.76 (m, 1H), 3.76–3.57 (m, 1H), 3.18–3.05 (m, 2H), 2.29–2.20 (m, 1H), 2.14 (ddd, *J* = 4.7, 11.2, 14.1 Hz, 1H), 1.97–1.89 (m, 1H), 1.78–1.64 (m, 4H), 1.64–1.51 (m, 1H), 1.43–1.35 (m, 1H), 0.93 (d, *J* = 6.4 Hz, 3H), 0.91 (d, *J* = 6.4 Hz, 3H).

To a solution of *N*-{[(2*S*)-4-chloro-3-oxo-1-[(3*S*)-2-oxopiperidin-3-yl]butan-2-yl]-*L*-leucinamide hydrochloride salt (2.30 g, 6.24 mmol) and 4-methoxy-1*H*-indole-2-carboxylic acid (1.31 g, 6.87 mmol) in anhydrous DMF (25 mL) cooled in an ice bath was added HATU (2.61 g, 6.87 mmol). Then, NMM (2.06 mL, 18.7 mmol) was added dropwise. After 45 min, the ice/saturated aqueous NaHCO₃ mixture (1:1, 150 mL) was added, and the resulting mixture was extracted

with EtOAc (3 × 150 mL). The combined organic layer was washed with saturated brine (1 × 150 mL), dried over anhydrous Na₂SO₄, filtered, and concentrated under reduced pressure. The residue was dissolved in CHCl₃ (25 mL), and the product was purified by silica gel column chromatography with a gradient of 0 to 4% MeOH in CHCl₃. The resulting solid was triturated with EtOAc (10 mL) and filtered, and the solid was washed with EtOAc (2 × 3 mL), then dried under vacuum, which generated 13 (1.71 g, 54% yield) as an off-white solid. *R*_f = 0.48 (5% MeOH in EtOAc) was a single spot under UV. ¹H NMR (600 MHz, DMSO-*d*₆) δ 11.57 (d, *J* = 2.1 Hz, 1H), 8.60 (d, *J* = 7.7 Hz, 1H), 8.44 (d, *J* = 7.5 Hz, 1H), 7.46 (br s, 1H), 7.37 (dd, *J* = 0.8, 2.3 Hz, 1H), 7.09 (t, *J* = 8.1 Hz, 1H), 7.02 (d, *J* = 8.3 Hz, 1H), 6.51 (d, *J* = 7.3 Hz, 1H), 4.61 (d, *J* = 16.0 Hz, 1H), 4.57 (d, *J* = 16.0 Hz, 1H), 4.53–4.42 (m, 2H), 3.89 (s, 3H), 3.13–3.04 (m, 2H), 2.22–2.13 (m, 2H), 1.89–1.80 (m, 1H), 1.78–1.66 (m, 4H), 1.60–1.47 (m, 2H), 1.39–1.29 (m, 1H), 0.95 (d, *J* = 6.4 Hz, 3H), 0.89 (d, *J* = 6.4 Hz, 3H). LC/MS: 5.19 min retention time, 98.2% pure. ESI-MS: 505 [M + H]⁺.

N-[(2*S*)-1-[(2*S*)-4-chloro-3-oxo-1-[(3*S*)-2-oxopyrrolidin-3-yl]butan-2-yl]amino)-4-methyl-1-oxopentan-2-yl]-4-methoxy-1*H*-indole-2-carboxamide (14). This material was prepared using the procedures in refs 11 and 39.

(3*S*)-3-[[*N*-(4-Methoxy-1*H*-indole-2-carbonyl)-*L*-leucyl]amino]-2-oxo-4-[(3*S*)-2-oxopiperidin-3-yl]butyl 2,2-Dimethylpropanoate (15a). A mixture of 2,2-dimethylpropanoic acid (10) (48.5 mg, 0.475 mmol) and sodium *tert*-butoxide (22.8 mg, 0.238 mmol) in anhydrous DMF (3 mL) was stirred at room temperature for 30 min. To this, 13 (40.0 mg, 0.079 mmol) and NaI (23.8 mg, 0.158 mmol) were added. After 24 h, a saturated brine solution (10 mL) was added, and the mixture extracted with CHCl₃ (3 × 10 mL). The combined organic layer was washed with saturated brine solution (10 mL), dried over anhydrous Na₂SO₄, filtered, and concentrated reduced pressure. The residue was dissolved in CHCl₃ (5 mL), and the product was purified by silica gel column chromatography with a gradient of 0 to 1% MeOH in CHCl₃, which afforded 15a (14.9 mg, 33% yield) as an off-white solid. *R*_f = 0.33 (5% MeOH in DCM). ¹H NMR (600 MHz, DMSO-*d*₆) δ 11.58 (d, *J* = 2.3 Hz, 1H), 8.57 (d, *J* = 8.1 Hz, 1H), 8.44 (d, *J* = 7.7 Hz, 1H), 7.46 (br s, 1H), 7.37 (dd, *J* = 0.8, 2.3 Hz, 1H), 7.11 (t, *J* = 8.0 Hz, 1H), 7.01 (d, *J* = 8.3 Hz, 1H), 6.51 (d, *J* = 7.5 Hz, 1H), 4.87 (d, *J* = 17.1 Hz, 1H), 4.84 (d, *J* = 17.1 Hz, 1H), 4.51–4.42 (m, 2H), 3.89 (s, 3H), 3.14–3.04 (m, 2H), 2.24–2.15 (m, 2H), 1.88–1.80 (m, 1H), 1.77–1.64 (m, 4H), 1.60–1.47 (m, 2H), 1.38–1.27 (m, 1H), 1.18 (s, 9H), 0.95 (d, *J* = 6.4 Hz, 3H), 0.90 (d, *J* = 6.4 Hz, 3H). ¹³C NMR (151 MHz, DMSO-*d*₆) δ 203.0, 176.8, 172.9, 172.6, 161.2, 153.6, 137.8, 129.8, 124.4, 118.0, 105.4, 101.2, 99.2, 66.3, 55.1, 53.2, 51.6, 41.2, 40.0, 36.8, 31.2, 30.4, 26.9 (3C), 25.6, 24.4, 23.0, 21.3, 21.2. LC/MS: 6.68 min retention time, 98.2% pure. Anal. Calcd for C₃₀H₄₂N₄O₇·0.25H₂O: C, 62.74; H, 7.44; N, 9.76. Found: C, 62.67; H, 7.46; N, 9.44. ESI-MS: 571 [M + H]⁺. HRMS (ESI+) calcd for C₃₀H₄₂N₄O₇ + H 571.3132, found 571.3153.

(3*S*)-3-[[*N*-(4-Methoxy-1*H*-indole-2-carbonyl)-*L*-leucyl]amino]-2-oxo-4-[(3*S*)-2-oxopiperidin-3-yl]butyl 2-Cyano-2-methylpropanoate (15b). The procedure for 15a was followed with 13 (40.0 mg, 0.0792 mmol), 2-cyano-2-methylpropanoic acid (60.7 mg, 0.537 mmol), sodium *tert*-butoxide (36.1 mg, 0.376 mmol), potassium iodide (47.4 mg, 0.286 mmol), and DMF (3 mL). The product was purified by column chromatography on silica gel (eluted with a gradient of 0–12% methanol in 1:1 chloroform/ethyl acetate mixture), followed by trituration with ether, which provided 15b (25.9 mg, 56% yield) as a white powder. *R*_f = 0.32 (5% MeOH in DCM). ¹H NMR (600 MHz, DMSO-*d*₆) δ 11.58 (d, *J* = 2.0 Hz, 1H), 8.68–8.58 (m, 1H), 8.45 (d, *J* = 7.6 Hz, 1H), 7.48–7.41 (m, 1H), 7.37 (dd, *J* = 0.7, 2.1 Hz, 1H), 7.10 (t, *J* = 8.1 Hz, 1H), 7.01 (d, *J* = 8.2 Hz, 1H), 6.51 (d, *J* = 7.6 Hz, 1H), 5.07 (d, *J* = 17.0 Hz, 1H), 5.01 (d, *J* = 17.0 Hz, 1H), 4.51–4.45 (m, 2H), 3.89 (s, 3H), 3.13–3.05 (m, 2H), 2.24–2.16 (m, 2H), 1.87–1.81 (m, 1H), 1.77–1.66 (m, 4H), 1.603 (s, 3H), 1.600 (s, 3H), 1.59–1.48 (m, 2H), 1.37–1.30 (m, 1H), 0.95 (d, *J* = 6.2 Hz, 3H), 0.90 (d, *J* = 6.2 Hz, 3H). LC/MS: 5.51 min retention time, 96.1% pure. ESI-MS 582 [M + H]⁺, 580 [M – H][–]. Anal. Calcd for C₃₀H₃₉N₅O₇·0.25H₂O: C, 61.74; H, 6.79; N,

11.95. Found: C, 61.49; H, 6.75; N, 11.78. HRMS (ESI+) calcd for $C_{30}H_{39}N_5O_7 + H$ 582.2928, found 582.2949.

(3S)-3-[[N-(4-methoxy-1H-indole-2-carbonyl)-L-leucyl]amino]-2-oxo-4-[(3S)-2-oxopiperidin-3-yl]butyl 3,3,3-Trifluoro-2,2-dimethylpropanoate (**15c**). The procedure for **15a** was followed with **13** (39.8 mg, 0.0789 mmol), 3,3,3-trifluoro-2,2-dimethylpropanoic acid (91.2 mg, 0.584 mmol), sodium *tert*-butoxide (42.2 mg, 0.439 mmol), potassium iodide (22.9 mg, 0.138 mmol), and DMF (3 mL). The product was purified by silica gel column chromatography (eluted with a gradient of 0–12% methanol in a 1:1 chloroform/ethyl acetate mixture) followed by trituration with ether, which provided **15c** (27.0 mg, 55% yield) as an off-white powder. $R_f = 0.34$ (5% MeOH in DCM). 1H NMR (600 MHz, DMSO- d_6) δ 11.58 (d, $J = 2.0$ Hz, 1H), 8.59 (d, $J = 8.1$ Hz, 1H), 8.45 (d, $J = 7.7$ Hz, 1H), 7.46 (brs, 1H), 7.37 (dd, $J = 0.7, 2.0$ Hz, 1H), 7.10 (dd, $J = 7.5, 8.2$ Hz, 1H), 7.01 (d, $J = 8.2$ Hz, 1H), 6.51 (d, $J = 7.6$ Hz, 1H), 5.00 (d, $J = 17.0$ Hz, 1H), 4.97 (d, $J = 17.0$ Hz, 1H), 4.50–4.44 (m, 2H), 3.89 (s, 3H), 3.12–3.05 (m, 2H), 2.24–2.16 (m, 2H), 1.87–1.81 (m, 1H), 1.76–1.66 (m, 4H), 1.59–1.48 (m, 2H), 1.42 (s, 6H), 1.37–1.30 (m, 1H), 0.95 (d, $J = 6.4$ Hz, 3H), 0.90 (d, $J = 6.4$ Hz, 3H). ^{13}C NMR (151 MHz, DMSO- d_6) δ 202.1, 173.0, 172.7, 169.0, 161.2, 153.7, 137.9, 129.9, 126.4 (q, $J = 281.9$ Hz, CF_3), 124.5, 118.1, 105.4, 101.2, 99.3, 67.5, 55.1, 53.2, 47.8 (q, $J = 23.3$ Hz), 51.7, 41.2, 40.1, 36.8, 31.1, 25.6, 24.5, 23.1, 21.3, 21.2, 19.3 (br, 2C). ^{19}F NMR (565 MHz, DMSO- d_6) δ -73.76 (s, 3F). LC/MS: 6.48 min retention time, 98.3% pure. ESI-MS 625 [M + H] $^+$, 623 [M - H] $^-$. HRMS (ESI+) calcd for $C_{30}H_{39}F_3N_4O_7 + H$ 625.2849, found 625.2861.

(3S)-3-[[N-(4-Methoxy-1H-indole-2-carbonyl)-L-leucyl]amino]-2-oxo-4-[(3S)-2-oxopiperidin-3-yl]butyl 2-Methyl-1,3-dioxane-2-carboxylate (**15d**). A mixture of 2-methyl-1,3-dioxane-2-carboxylic acid (69.5 mg, 0.475 mmol) (prepared following the procedure in ref 57) and sodium *tert*-butoxide (22.8 mg, 0.238 mmol) in anhydrous DMF (3 mL) was stirred at room temperature for 30 min. To this, **13** (40.1 mg, 0.079 mmol) and NaI (23.8 mg, 0.158 mmol) were added successively. After 24 h, saturated brine (10 mL) was added, and the resulting mixture was extracted with $CHCl_3$ (3 \times 10 mL). The combined organic layer was washed with saturated brine solution (1 \times 10 mL), dried over anhydrous Na_2SO_4 , filtered, and concentrated under reduced pressure. The residue was dissolved in $CHCl_3$ (5 mL), and the product was purified by silica gel column chromatography with a gradient of 0–4% MeOH in DCM, which afforded **15d** (24.9 mg, 51% yield) as an off-white solid. $R_f = 0.34$ (5% MeOH in DCM). 1H NMR (600 MHz, DMSO- d_6) δ 11.58 (d, $J = 2.1$ Hz, 1H), 8.60 (d, $J = 8.1$ Hz, 1H), 8.45 (d, $J = 7.5$ Hz, 1H), 7.46 (br s, 1H), 7.38 (dd, $J = 0.8, 2.3$ Hz, 1H), 7.11 (t, $J = 8.1$ Hz, 1H), 7.01 (d, $J = 8.3$ Hz, 1H), 6.51 (d, $J = 7.3$ Hz, 1H), 5.05 (d, $J = 17.1$ Hz, 1H), 5.01 (d, $J = 17.1$ Hz, 1H), 4.54–4.45 (m, 2H), 3.89 (s, 3H), 3.88–3.79 (m, 4H), 3.14–3.05 (m, 2H), 2.26–2.17 (m, 2H), 1.94–1.81 (m, 2H), 1.79–1.66 (m, 4H), 1.62–1.46 (m, 2H), 1.38 (s, 3H), 1.36–1.19 (m, 2H), 0.95 (d, $J = 6.4$ Hz, 3H), 0.90 (d, $J = 6.4$ Hz, 3H). ^{13}C NMR (151 MHz, DMSO- d_6) δ 202.8, 173.0, 172.6, 169.5, 161.2, 153.6, 137.8, 129.8, 124.4, 118.1, 105.4, 101.2, 99.2, 97.8, 67.2, 62.3 (2C), 55.1, 53.3, 51.7, 41.2, 40.1, 36.8, 31.2, 26.2, 25.6, 24.4, 24.1, 23.0, 21.3, 21.2. LC/MS: 6.69 min retention time, 99.1% pure. ESI-MS: 615 [M + H] $^+$. Anal. Calcd for $C_{31}H_{42}N_4O_9 \cdot 0.1H_2O$: C, 60.40; H, 6.90; N, 9.09. Found: C, 60.45; H, 6.92; N, 8.94. HRMS (ESI+) calcd for $C_{31}H_{42}N_4O_9 + H$ 615.3030, found 615.3049.

(3S)-3-[[N-(4-Methoxy-1H-indole-2-carbonyl)-L-leucyl]amino]-2-oxo-4-[(3S)-2-oxopiperidin-3-yl]butyl 1-(Trifluoromethyl)cyclohexane-1-carboxylate (**15e**). The procedure for **15a** was followed with **13** (50.1 mg, 0.0992 mmol), 1-(trifluoromethyl)cyclohexanecarboxylic acid (105.1 mg, 0.536 mmol), sodium *tert*-butoxide (44.3 mg, 0.461 mmol), potassium iodide (102 mg, 0.614 mmol), and DMF (3 mL). The product was purified by column chromatography (eluted with a gradient of 0–12% methanol in a 1:1 chloroform/ethyl acetate mixture) followed by trituration with ether, which provided **15e** (9.6 mg, 15% yield) as a yellow powder. $R_f = 0.46$ (5% MeOH in DCM). 1H NMR (600 MHz, DMSO- d_6) δ 11.56 (br s, 1H), 8.65–8.30 (m, 2H), 7.48–7.32 (m, 2H), 7.10 (dd, $J = 7.8, 8.0$ Hz, 1H), 7.01 (d, $J = 8.1$ Hz, 1H), 6.51 (d, $J = 7.6$ Hz, 1H), 5.10–

4.98 (m, 2H), 4.63–4.44 (m, 2H), 3.89 (s, 3H), 3.13–3.04 (m, 2H), 2.25–2.12 (m, 4H), 1.87–1.15 (m, 16H), 0.94 (d, $J = 6.0$ Hz, 3H), 0.89 (d, $J = 6.0$ Hz, 3H). ^{13}C NMR (151 MHz, DMSO- d_6) δ 202.1, 173.3, 172.8, 167.5, 161.3, 153.7, 137.9, 129.9, 125.8 (q, $J = 283.3$ Hz, CF_3), 124.5, 118.1, 105.5, 101.3, 99.3, 67.9, 55.1, 53.3, 52.5 (q, $J = 23.3$ Hz), 51.7, 41.3, 40.1, 36.9, 31.2, 27.11, 27.06, 25.6, 24.5, 24.2, 23.1, 21.46, 21.44, 21.37, 21.2. ^{19}F NMR (565 MHz, DMSO- d_6) δ -73.56 (s, 3F). LC/MS: 7.04 min retention time, 97.5% pure. ESI-MS 665 [M + H] $^+$, 663 [M - H] $^-$. Anal. Calcd for $C_{33}H_{43}F_3N_4O_7 \cdot 0.2H_2O$: C, 59.31; H, 6.55; N, 8.38. Found: C, 59.39; H, 6.53; N, 8.28. HRMS (ESI+) calcd for $C_{33}H_{43}F_3N_4O_7 + H$ 665.3162, found 665.3197.

(3S)-3-[[N-(4-Methoxy-1H-indole-2-carbonyl)-L-leucyl]amino]-2-oxo-4-[(3S)-2-oxopiperidin-3-yl]butyl Benzoate (**15f**). To a solution of benzoic acid (37.1 mg, 0.303 mmol) in DMF (3 mL) was added sodium *tert*-butoxide (19.2 mg, 0.199 mmol). After 15 min, a solution of **13** (50.1 mg, 0.099 mmol) in DMF (2 mL) was added followed by NaI (14.9 mg, 0.099 mmol), and the solution was allowed to sit overnight. Water (5 mL) was then added, and the resulting mixture was extracted with DCM (3 \times 25 mL). The combined organic phase was washed with brine (10 mL), dried over Na_2SO_4 , filtered, and concentrated under reduced pressure. The product was purified by column chromatography on silica gel with a gradient of 0–10% MeOH in EtOAc, which generated **15f** (15 mg, 25% yield) as a white solid. $R_f = 0.31$ (5% MeOH in DCM). 1H NMR (600 MHz, DMSO- d_6) δ 11.58 (d, $J = 2.3$ Hz, 1H), 8.64 (d, $J = 7.9$ Hz, 1H), 8.45 (d, $J = 7.5$ Hz, 1H), 8.01–7.96 (m, 2H), 7.71–7.68 (m, 1H), 7.59–7.52 (m, 2H), 7.47 (br s, 1H), 7.39–7.36 (m, 1H), 7.12–7.07 (m, 1H), 7.03–6.99 (m, 1H), 6.51 (d, $J = 7.5$ Hz, 1H), 5.16–5.11 (m, 2H), 4.56–4.46 (m, 2H), 3.88 (s, 3H), 3.13–3.06 (m, 2H), 2.27–2.19 (m, 2H), 1.88–1.82 (m, 1H), 1.79–1.66 (m, 4H), 1.62–1.48 (m, 2H), 1.38–1.32 (m, 1H), 0.95 (d, $J = 6.4$ Hz, 3H), 0.90 (d, $J = 6.4$ Hz, 3H). ^{13}C NMR (151 MHz, DMSO- d_6) δ 202.9, 173.0, 172.6, 165.0, 161.2, 153.6, 137.8, 133.7, 129.9, 129.3 (2C), 129.0, 128.9 (2C), 124.4, 118.1, 105.4, 101.2, 99.2, 67.1, 55.1, 53.3, 51.7, 41.2, 40.1, 36.9, 31.2, 25.6, 24.4, 23.0, 21.4, 21.2. LC/MS: 6.19 min retention time, 98.3% pure. ESI-MS 591 [M + H] $^+$. HRMS (ESI+) calcd for $C_{32}H_{38}N_4O_7 + H$ 591.2819, found 591.2825.

(3S)-3-[[N-(4-Methoxy-1H-indole-2-carbonyl)-L-leucyl]amino]-2-oxo-4-[(3S)-2-oxopiperidin-3-yl]butyl 2,6-Dichlorobenzoate (**15g**). After 30 min, to a solution of 2,6-dichlorobenzoic acid (101 mg, 0.529 mmol) and sodium *tert*-butoxide (29.7 mg, 0.309 mmol) in DMF (3 mL) was added **13** (49.8 mg, 0.0986 mmol) followed by potassium iodide (41.6 mg, 0.251 mmol), and the solution was allowed to sit overnight. The mixture was then diluted with DCM (15 mL) and washed with water (15 mL). The organic layer was poured into a Petri dish and left in the fume hood to dry. The residue was dissolved in a minimal amount of ethyl acetate and loaded on silica. Purification of the product by silica gel column chromatography (eluted with a gradient of 0–12% methanol in a 1:1 chloroform/ethyl acetate mixture) followed by recrystallization from ethyl acetate provided **15g** (17.8 mg, 27% yield) as a white powder. $R_f = 0.46$ (5% MeOH in DCM). 1H NMR (600 MHz, DMSO- d_6) δ 11.55 (d, $J = 2.1$ Hz, 1H), 8.62 (d, $J = 7.6$ Hz, 1H), 8.45 (d, $J = 7.6$ Hz, 1H), 7.62–7.59 (m, 2H), 7.57–7.54 (m, 1H), 7.47–7.44 (m, 1H), 7.36 (dd, $J = 0.9, 2.3$ Hz, 1H), 7.10 (t, $J = 8.0$ Hz, 1H), 7.01 (d, $J = 8.3$ Hz, 1H), 6.51 (d, $J = 8.0$ Hz, 1H), 5.19 (d, $J = 17.0$ Hz, 1H), 5.16 (d, $J = 17.0$ Hz, 1H), 4.58–4.48 (m, 2H), 3.88 (s, 3H), 3.12–3.04 (m, 2H), 2.25–2.20 (m, 2H), 1.87–1.66 (m, 4H), 1.61–1.47 (m, 2H), 1.38–1.31 (m, 2H), 0.95 (d, $J = 6.3$ Hz, 3H), 0.90 (d, $J = 6.6$ Hz, 3H). ^{13}C NMR (151 MHz, DMSO- d_6) δ 201.4, 173.1, 172.8, 163.4, 161.2, 153.7, 137.9, 132.7, 132.1, 130.9 (2C), 129.9, 128.6 (2C), 124.5, 118.1, 105.5, 101.3, 99.3, 67.9, 55.1, 53.3, 51.7, 41.3, 40.1, 36.9, 31.1, 25.6, 24.5, 23.0, 21.5, 21.2. LC/MS: 6.33 min retention time, 96.8% pure. ESI-MS 659 [M + H] $^+$, 657 [M - H] $^-$. HRMS (ESI+) calcd for $C_{32}H_{36}Cl_2N_4O_7 + H$ 659.2039, found 659.2070.

(3S)-3-[[N-(4-Methoxy-1H-indole-2-carbonyl)-L-leucyl]amino]-2-oxo-4-[(3S)-2-oxopiperidin-3-yl]butyl 2,6-Bis(trifluoromethyl)benzoate (**15h**). A mixture of 2,6-bis(trifluoromethyl)benzoic acid (122.7 mg, 0.475 mmol) and sodium *tert*-butoxide (22.8 mg, 0.238

mmol) in anhydrous DMF (3 mL) was stirred at room temperature for 30 min. To this, **13** (40.0 mg, 0.079 mmol) and NaI (23.8 mg, 0.158 mmol) were added successively. After 48 h, a saturated brine solution (10 mL) was added, and the mixture was extracted with CHCl₃ (3 × 10 mL). The combined organic layer was washed with saturated brine solution (10 mL), dried over anhydrous Na₂SO₄, filtered, and concentrated under reduced pressure. The resulting residue was dissolved in CHCl₃ (5 mL) and loaded on a silica gel column, and the product was purified with a gradient of 0–2% MeOH in CHCl₃, which afforded **15h** (31.9 mg, 55% yield) as an off-white solid. *R*_f = 0.40 (5% MeOH in DCM). ¹H NMR (600 MHz, DMSO-*d*₆) δ 11.55 (d, *J* = 2.1 Hz, 1H), 8.65 (d, *J* = 7.9 Hz, 1H), 8.45 (d, *J* = 7.7 Hz, 1H), 8.26 (d, *J* = 7.9 Hz, 2H), 8.02 (t, *J* = 8.0 Hz, 1H), 7.46 (br s, 1H), 7.37 (dd, *J* = 0.7, 2.2 Hz, 1H), 7.11 (t, *J* = 8.1 Hz, 1H), 7.02 (d, *J* = 8.2 Hz, 1H), 6.51 (d, *J* = 7.5 Hz, 1H), 5.21 (d, *J* = 17.1 Hz, 1H), 5.16 (d, *J* = 17.1 Hz, 1H), 4.60–4.49 (m, 2H), 3.89 (s, 3H), 3.15–3.03 (m, 2H), 2.28–2.19 (m, 2H), 1.87–1.79 (m, 1H), 1.77–1.63 (m, 4H), 1.62–1.55 (m, 1H), 1.55–1.46 (m, 1H), 1.37–1.28 (m, 1H), 0.95 (d, *J* = 6.4 Hz, 3H), 0.90 (d, *J* = 6.4 Hz, 3H). ¹³C NMR (151 MHz, DMSO-*d*₆) δ 200.8, 172.94, 172.6, 163.9, 161.1, 153.6, 137.8, 132.2, 131.0 (q, *J* = 4.2 Hz, 2C), 129.8, 128.7 (q, *J* = 2.1 Hz), 127.4 (q, *J* = 32.2 Hz, 2C), 124.4, 122.7 (q, *J* = 274.3 Hz, 2C), 118.1, 105.4, 101.2, 99.2, 68.2, 55.1, 53.1, 51.4, 41.2, 40.1, 36.8, 30.9, 25.6, 24.4, 22.9, 21.4, 21.1. ¹⁹F NMR (565 MHz, DMSO-*d*₆) δ –58.28 to –58.36 (m, 6F). LC/MS: 6.49 min retention time, 97.1% pure. ESI-MS: 727 [M + H]⁺. HRMS (ESI+) calcd for C₃₄H₃₆F₆N₄O₇ + H 727.2567, found 727.2592.

(3*S*)-3-[[*N*-(4-Methoxy-1*H*-indole-2-carbonyl)-*L*-leucyl]amino]-2-oxo-4-[(3*S*)-2-oxopiperidin-3-yl]butylpyridine-2-carboxylate (**15i**). To a solution of picolinic acid (41.1 mg, 0.333 mmol) in DMF (3 mL) was added sodium *tert*-butoxide (21.2 mg, 0.221 mmol). After 15 min, a solution of **13** (54.9 mg, 0.108 mmol) in DMF (2 mL) was added followed by the addition of NaI (16.0 mg, 0.107 mmol). The reaction mixture was stirred at room temperature overnight. Then, it was quenched by adding water (5 mL). The mixture was extracted with DCM (3 × 25 mL), and the combined organic phase was washed with brine (10 mL), dried over Na₂SO₄, filtered, and concentrated. The product was purified by column chromatography on silica gel with a gradient of 0–10% MeOH in EtOAc, which generated **15i** (12 mg, 20% yield) as a white solid. *R*_f = 0.21 (5% MeOH in DCM). ¹H NMR (600 MHz, DMSO-*d*₆) δ 11.59 (d, *J* = 1.9 Hz, 1H), 8.77–8.73 (m, 1H), 8.65 (d, *J* = 8.3 Hz, 1H), 8.46 (d, *J* = 7.5 Hz, 1H), 8.11–8.07 (m, 1H), 8.05–8.00 (m, 1H), 7.69 (ddd, *J* = 1.1, 4.7, 7.7 Hz, 1H), 7.47 (br s, 1H), 7.39–7.37 (m, 1H), 7.12–7.07 (m, 1H), 7.03–6.99 (m, 1H), 6.51 (d, *J* = 7.5 Hz, 1H), 5.22–5.13 (m, 2H), 4.58–4.53 (m, 1H), 4.52–4.46 (m, 1H), 3.89 (s, 3H), 3.13–3.06 (m, 2H), 2.28–2.21 (m, 2H), 1.89–1.83 (m, 1H), 1.78–1.68 (m, 4H), 1.62–1.48 (m, 2H), 1.40–1.33 (m, 1H), 0.96 (d, *J* = 6.4 Hz, 3H), 0.91 (d, *J* = 6.4 Hz, 3H). LC/MS: 5.19 min retention time, 96.2% pure. ESI-MS 592 [M + H]⁺. HRMS (ESI+) calcd for C₃₁H₃₇N₅O₇ + H 592.2771, found 592.2782.

(3*S*)-3-[[*N*-(4-Methoxy-1*H*-indole-2-carbonyl)-*L*-leucyl]amino]-2-oxo-4-[(3*S*)-2-oxopiperidin-3-yl]butylpyridine-3-carboxylate (**15j**). To a solution of nicotinic acid (37.0 mg, 0.301 mmol) in DMF (3 mL) was added sodium *tert*-butoxide (19.2 mg, 0.200 mmol). After 15 min, a solution of **13** (50.3 mg, 0.100 mmol) in DMF (2 mL) was added followed by the addition of NaI (15 mg, 0.10 mmol), and the solution was allowed to sit overnight. Water (5 mL) was then added, and the resulting mixture was extracted with DCM (3 × 25 mL). The combined organic layer was washed with brine (10 mL), dried over Na₂SO₄, filtered, and concentrated under reduced pressure. The product was purified by column chromatography on silica gel with a gradient of 0–10% MeOH in EtOAc, which generated **15j** (28 mg, 47% yield) as an off-white solid. *R*_f = 0.25 (5% MeOH in DCM). ¹H NMR (600 MHz, DMSO-*d*₆) δ 11.58 (d, *J* = 2.2 Hz, 1H), 9.12 (dd, *J* = 0.8, 2.3 Hz, 1H), 8.86 (dd, *J* = 1.5, 4.9 Hz, 1H), 8.65 (d, *J* = 8.3 Hz, 1H), 8.46 (d, *J* = 7.5 Hz, 1H), 8.34–8.31 (m, 1H), 7.61 (ddd, *J* = 1.1, 4.8, 8.0 Hz, 1H), 7.48 (br s, 1H), 7.40–7.37 (m, 1H), 7.13–7.08 (m, 1H), 7.03–6.99 (m, 1H), 6.51 (d, *J* = 7.5 Hz, 1H), 5.21–5.13 (m, 2H), 4.59–4.52 (m, 1H), 4.52–4.47 (m, 1H), 3.89 (s, 3H), 3.13–

3.06 (m, 2H), 2.27–2.21 (m, 2H), 1.89–1.83 (m, 1H), 1.78–1.67 (m, 4H), 1.61–1.48 (m, 2H), 1.39–1.31 (m, 1H), 0.95 (d, *J* = 6.4 Hz, 3H), 0.90 (d, *J* = 6.8 Hz, 3H). LC/MS: 5.31 min retention time, 95.9% pure. ESI-MS 592 [M + H]⁺. HRMS (ESI+) calcd for C₃₁H₃₇N₅O₇ + H 592.2771, found 592.2795.

(3*S*)-3-[[*N*-(4-Methoxy-1*H*-indole-2-carbonyl)-*L*-leucyl]amino]-2-oxo-4-[(3*S*)-2-oxopiperidin-3-yl]butylpyridine-4-carboxylate (**15k**). To a solution of isonicotinic acid (37.1 mg, 0.301 mmol) in DMF (5 mL) was added sodium *tert*-butoxide (19.2 mg, 0.200 mmol). After 15 min, **13** (50.0 mg, 0.099 mmol) was added followed by KI (16.6 mg, 0.100 mmol). After 2 days, water (5 mL) was added, and the resulting mixture was extracted with EtOAc (3 × 20 mL). The combined organic phase was washed with brine (10 mL), dried over Na₂SO₄, filtered, and concentrated under reduced pressure. The product was purified by column chromatography on silica gel with a gradient of 0–10% MeOH in EtOAc, which generated **15k** (31 mg, 52% yield) as a white solid. *R*_f = 0.32 (5% MeOH in DCM). ¹H NMR (600 MHz, DMSO-*d*₆) δ 11.58 (d, *J* = 2.3 Hz, 1H), 8.88–8.81 (m, 2H), 8.65 (d, *J* = 7.9 Hz, 1H), 8.46 (d, *J* = 7.9 Hz, 1H), 7.89–7.84 (m, 2H), 7.48 (br s, 1H), 7.39–7.37 (m, 1H), 7.13–7.08 (m, 1H), 7.04–6.99 (m, 1H), 6.52 (d, *J* = 7.5 Hz, 1H), 5.23–5.15 (m, 2H), 4.58–4.52 (m, 1H), 4.52–4.46 (m, 1H), 3.89 (s, 3H), 3.14–3.06 (m, 2H), 2.27–2.20 (m, 2H), 1.89–1.83 (m, 1H), 1.80–1.64 (m, 4H), 1.61–1.50 (m, 2H), 1.39–1.31 (m, 1H), 0.95 (d, *J* = 6.4 Hz, 3H), 0.90 (d, *J* = 6.4 Hz, 3H). LC/MS: 5.36 min retention time, 95.4% pure. ESI-MS 592 [M + H]⁺. HRMS (ESI+) calcd for C₃₁H₃₇N₅O₇ + H 592.2771, found 592.2797.

(3*S*)-3-[[*N*-(4-Methoxy-1*H*-indole-2-carbonyl)-*L*-leucyl]amino]-2-oxo-4-[(3*S*)-2-oxopiperidin-3-yl]butyl 2,4,6-Trimethylpyridine-3-carboxylate (**15l**). To a solution of 2,4,6-trimethylpyridine-3-carboxylic acid hydrochloride (81.3 mg, 0.403 mmol) in DMF (5 mL) was added sodium *tert*-butoxide (58.0 mg, 0.603 mmol). After 30 min, **13** (50.8 mg, 0.101 mmol) and then KI (16.6 mg, 0.100 mmol) was added. After 2 days, EtOAc (40 mL) was added, and the mixture was washed with water (3 × 10 mL) and brine (10 mL), dried over Na₂SO₄, filtered, and concentrated under reduced pressure. The product was purified by column chromatography on silica gel with a gradient of 0–10% MeOH in CHCl₃, which generated **15l** (38 mg, 60% yield) as a white solid. *R*_f = 0.31 (5% MeOH in DCM). ¹H NMR (600 MHz, DMSO-*d*₆) δ 11.57 (d, *J* = 2.3 Hz, 1H), 8.63 (d, *J* = 8.3 Hz, 1H), 8.45 (d, *J* = 7.9 Hz, 1H), 7.46 (br s, 1H), 7.39–7.36 (m, 1H), 7.12–7.08 (m, 1H), 7.05–7.00 (m, 2H), 6.51 (d, *J* = 7.2 Hz, 1H), 5.18–5.09 (m, 2H), 4.57–4.49 (m, 2H), 3.89 (s, 3H), 3.13–3.06 (m, 2H), 2.46 (s, 3H), 2.41 (s, 3H), 2.30 (s, 3H), 2.28–2.21 (m, 2H), 1.89–1.83 (m, 1H), 1.78–1.68 (m, 4H), 1.63–1.49 (m, 2H), 1.39–1.32 (m, 1H), 0.96 (d, *J* = 6.4 Hz, 3H), 0.91 (d, *J* = 6.4 Hz, 3H). ¹³C NMR (151 MHz, DMSO-*d*₆) δ 202.8, 173.0, 172.6, 167.4, 161.2, 158.4, 154.2, 153.6, 145.2, 137.8, 129.8, 125.3, 124.4, 122.0, 118.1, 105.4, 101.2, 99.2, 67.3, 55.1, 53.3, 51.7, 41.2, 40.0, 36.8, 31.2, 25.6, 24.4, 23.8, 23.0, 22.7, 21.4, 21.2, 19.0. LC/MS: 4.39 min retention time, 99.5% pure. ESI-MS 634 [M + H]⁺. Anal. Calcd for C₃₄H₄₃N₅O₇·0.35H₂O: C, 63.80; H, 6.88; N, 10.94. Found: C, 63.85; H, 6.93; N, 10.85. HRMS (ESI+) calcd for C₃₄H₄₃N₅O₇ + H 634.3241, found 634.3239.

(3*S*)-3-[[*N*-(4-Methoxy-1*H*-indole-2-carbonyl)-*L*-leucyl]amino]-2-oxo-4-[(3*S*)-2-oxopiperidin-3-yl]butyl 2,6-Dimethyl-4-(trifluoromethyl)pyridine-3-carboxylate (**15m**). To a solution of 2,6-dimethyl-4-(trifluoromethyl)pyridine-3-carboxylic acid hydrochloride (102 mg, 0.400 mmol) (prepared using the procedures in refs **58** and **59**) in DMF (5 mL) was added sodium *tert*-butoxide (58.1 mg, 0.605 mmol). After 30 min, **13** (50.1 mg, 0.099 mmol) followed by KI (16.6 mg, 0.100 mmol) was added. After 3 days, EtOAc (40 mL) was added, and the mixture was washed with water (3 × 10 mL) and brine (10 mL), dried over Na₂SO₄, filtered, and concentrated under reduced pressure. The product was purified by column chromatography on silica gel with a gradient of 0–10% MeOH in CHCl₃, which generated **15m** (23 mg, 33% yield) as a white solid. *R*_f = 0.36 (5% MeOH in DCM). ¹H NMR (600 MHz, DMSO-*d*₆) δ 11.56 (d, *J* = 2.3 Hz, 1H), 8.64 (d, *J* = 8.3 Hz, 1H), 8.45 (d, *J* = 7.5 Hz, 1H), 7.63 (s, 1H), 7.47 (br s, 1H), 7.38–7.36 (m, 1H),

7.12–7.08 (m, 1H), 7.03–6.99 (m, 1H), 6.51 (d, $J = 7.2$ Hz, 1H), 5.23–5.13 (m, 2H), 4.60–4.48 (m, 2H), 3.89 (s, 3H), 3.13–3.05 (m, 2H), 2.63 (s, 3H), 2.59 (s, 3H), 2.29–2.20 (m, 2H), 1.89–1.82 (m, 1H), 1.79–1.66 (m, 4H), 1.63–1.48 (m, 2H), 1.40–1.32 (m, 1H), 0.95 (d, $J = 6.4$ Hz, 3H), 0.90 (d, $J = 6.4$ Hz, 3H). ^{13}C NMR (151 MHz, DMSO- d_6) δ 202.1, 173.0, 172.6, 165.5, 161.2, 161.1, 156.0, 153.6, 137.8, 134.2 (q , $J = 32.6$ Hz), 129.8, 124.40, 122.4 (q , $J = 274.7$ Hz), 121.4, 118.1, 116.8 (q , $J = 4.5$ Hz), 105.4, 101.2, 99.2, 67.9, 55.1, 53.2, 51.6, 41.2, 40.0, 36.8, 31.1, 25.6, 24.4, 24.0, 23.0, 22.4, 21.4, 21.2. ^{19}F NMR (565 MHz, DMSO- d_6) δ -60.74 (s, 3F). LC/MS: 6.37 min retention time, 96.9% pure. ESI-MS 688 $[\text{M} + \text{H}]^+$. HRMS (ESI+) calcd for $\text{C}_{34}\text{H}_{40}\text{F}_3\text{N}_5\text{O}_7 + \text{H}$ 688.2958, found 688.2975.

(3S)-3-[[N-(4-Methoxy-1H-indole-2-carbonyl)-L-leucyl]amino]-2-oxo-4-[(3S)-2-oxopiperidin-3-yl]butyl 2,4,6-Trimethylpyrimidine-5-carboxylate (15n). To 2,4,6-trimethylpyrimidine-5-carboxylic acid (82.3 mg, 0.495 mmol) in anhydrous DMF (3 mL) was added sodium *tert*-butoxide (23.8 mg, 0.247 mmol). After 30 min, 13 (50.1 mg, 0.099 mmol) and NaI (29.7 mg, 0.198 mmol) were added, and the solution was allowed to sit overnight. Saturated brine (10 mL) was then added, and the resulting mixture was extracted with CHCl_3 (3×10 mL). The combined organic layer was washed with saturated brine solution (1×10 mL), dried over anhydrous Na_2SO_4 , filtered, and concentrated under reduced pressure. The residue was dissolved in CHCl_3 (5 mL) and loaded on a silica gel column, and the product was purified by silica gel column chromatography with a gradient of 0–6% MeOH in CHCl_3 , which afforded 15n (38.1 mg, 61% yield) as an off-white solid. $R_f = 0.21$ (5% MeOH in DCM). ^1H NMR (600 MHz, DMSO- d_6) δ 11.57 (d, $J = 2.3$ Hz, 1H), 8.64 (d, $J = 8.1$ Hz, 1H), 8.46 (d, $J = 7.5$ Hz, 1H), 7.48–7.45 (m, 1H), 7.38 (dd, $J = 0.8, 2.3$ Hz, 1H), 7.12–7.08 (m, 1H), 7.01 (d, $J = 8.1$ Hz, 1H), 6.51 (d, $J = 7.3$ Hz, 1H), 5.23–5.14 (m, 2H), 4.59–4.53 (m, 1H), 4.53–4.48 (m, 1H), 3.89 (s, 3H), 3.14–3.05 (m, 2H), 2.57 (s, 3H), 2.49 (s, 6H), 2.28–2.20 (m, 2H), 1.90–1.81 (m, 1H), 1.79–1.67 (m, 4H), 1.63–1.48 (m, 2H), 1.41–1.31 (m, 1H), 0.96 (d, $J = 6.4$ Hz, 3H), 0.91 (d, $J = 6.4$ Hz, 3H). ^{13}C NMR (151 MHz, DMSO- d_6) δ 202.7, 173.0, 172.6, 167.2, 166.3, 164.2, 161.2, 153.6, 137.8, 129.8, 124.4, 122.3, 118.0, 105.4, 101.2, 99.2, 67.7, 55.1, 53.3, 51.7, 41.2, 40.1, 40.0, 36.8, 31.2, 25.6, 25.5, 24.4, 23.0, 22.43 (2C), 21.37, 21.2. LC/MS: 5.71 min retention time, 98.5% pure. ESI-MS: 635 $[\text{M} + \text{H}]^+$; Anal. Calcd for $\text{C}_{33}\text{H}_{43}\text{N}_6\text{O}_7 \cdot 0.35\text{H}_2\text{O}$: C, 61.83; H, 6.71; N, 13.11. Found: C, 61.80; H, 6.61; N, 12.92. HRMS (ESI+) calcd for $\text{C}_{33}\text{H}_{42}\text{N}_6\text{O}_7 + \text{H}$ 635.3193, found 635.3210.

(3S)-3-[[N-(4-Methoxy-1H-indole-2-carbonyl)-L-leucyl]amino]-2-oxo-4-[(3S)-2-oxopiperidin-3-yl]butyl 1,3,5-Trimethyl-1H-pyrazole-4-carboxylate (15o). To a solution of 1,3,5-trimethyl-1H-pyrazole-4-carboxylic acid (55.1 mg, 0.357 mmol) in DMF (1 mL) was added sodium *tert*-butoxide (17.1 mg, 0.178 mmol). After 10 min, 13 (45.0 mg, 0.0891 mmol) was added to the mixture followed by sodium iodide (26.7 mg, 0.178 mmol), and the solution was allowed to sit overnight. The mixture was then diluted with ethyl acetate/chloroform (75 mL/25 mL), and the resulting mixture was washed with water (25 mL) and brine (25 mL), dried over MgSO_4 , and concentrated under reduced pressure. The product was purified by column chromatography on silica with a gradient of 0 to 2% methanol in 1:1 chloroform/ethyl acetate, which generated 15o (13.0 mg, 23% yield) as white solid. $R_f = 0.25$ (5% MeOH in DCM). ^1H NMR (600 MHz, DMSO- d_6) δ 11.57 (d, $J = 2.1$ Hz, 1H), 8.60 (d, $J = 8.3$ Hz, 1H), 8.44 (d, $J = 8.3$ Hz, 1H), 7.45 (br s, 1H), 7.37 (dd, $J = 0.8, 2.3$ Hz, 1H), 7.15–7.07 (m, 1H), 7.04–6.97 (m, 1H), 6.51 (d, $J = 7.9$ Hz, 1H), 5.09–4.94 (m, 2H), 4.56–4.44 (m, 2H), 3.89 (s, 3H), 3.69 (s, 3H), 2.44 (s, 3H), 2.26 (s, 3H), 1.92–1.78 (m, 2H), 1.78–1.65 (m, 4H), 1.62–1.46 (m, 4H), 1.43–1.25 (m, 2H), 0.95 (d, $J = 6.0$ Hz, 3H), 0.91 (d, $J = 6.0$ Hz, 3H). ^{13}C NMR (151 MHz, DMSO- d_6) δ 203.8, 173.4, 173.2, 163.2, 161.6, 154.1, 149.2, 144.6, 138.3, 130.3, 124.9, 118.5, 108.29, 108.27, 105.9, 101.7, 99.7, 66.2, 55.5, 53.7, 52.1, 41.7, 37.3, 36.3, 31.7, 26.1, 24.9, 23.5, 21.8, 21.6, 14.3, 11.3. LC/MS: 5.53 min retention time, 96.5% pure. ESI-MS: 623 $[\text{M} + \text{H}]^+$. HRMS (ESI+) calcd for $\text{C}_{32}\text{H}_{42}\text{N}_6\text{O}_7 + \text{H}$ 623.3193, found 623.3232.

(3S)-3-[[N-(4-Methoxy-1H-indole-2-carbonyl)-L-leucyl]amino]-2-oxo-4-[(3S)-2-oxopyrrolidin-3-yl]butyl 2,6-Dimethyl-4-

(trifluoromethyl)pyridine-3-carboxylate (16m). To a solution of 2,6-dimethyl-4-(trifluoromethyl)pyridine-3-carboxylic acid hydrochloride (102.4 mg, 0.401 mmol) (prepared using the procedures in refs 58 and 59) in DMF (5 mL) was added sodium *tert*-butoxide (58.5 mg, 0.609 mmol). After 30 min, 14 (50.4 mg, 0.103 mmol) followed by KI (16.6 mg, 0.100 mmol) was added. After 3 days, EtOAc (40 mL) was added, and the resulting mixture was washed with water (3×10 mL) and brine (10 mL), dried over Na_2SO_4 , filtered, and concentrated under reduced pressure. The product was purified by column chromatography on silica gel with a gradient of 0–10% MeOH in CHCl_3 , which generated 16m (32 mg, 47% yield) as a white solid. $R_f = 0.34$ (5% MeOH in DCM). ^1H NMR (600 MHz, DMSO- d_6) δ 11.57 (d, $J = 2.3$ Hz, 1H), 8.65 (d, $J = 7.9$ Hz, 1H), 8.46 (d, $J = 7.9$ Hz, 1H), 7.66 (s, 1H), 7.63 (s, 1H), 7.39–7.36 (m, 1H), 7.14–7.07 (m, 1H), 7.04–6.98 (m, 1H), 6.51 (d, $J = 7.2$ Hz, 1H), 5.23–5.14 (m, 2H), 4.57–4.49 (m, 2H), 3.89 (s, 3H), 3.18–3.06 (m, 2H), 2.64 (s, 3H), 2.59 (s, 3H), 2.39–2.31 (m, 1H), 2.14–2.01 (m, 2H), 1.77–1.57 (m, 5H), 0.95 (d, $J = 6.4$ Hz, 3H), 0.91 (d, $J = 6.4$ Hz, 3H). ^{13}C NMR (151 MHz, DMSO- d_6) δ 201.8, 178.3, 173.1, 165.5, 161.2, 161.2, 156.04, 153.6, 137.8, 134.2 (q , $J = 33.0$ Hz), 129.8, 124.4, 122.4 (q , $J = 274.4$ Hz), 121.4, 118.1, 116.8 (q , $J = 4.1$ Hz), 105.4, 101.2, 99.2, 67.8, 55.1, 54.9, 53.9, 51.6, 40.0, 37.3, 30.7, 27.1, 24.4, 24.0, 23.0, 22.4, 21.3. ^{19}F NMR (565 MHz, DMSO- d_6) δ -60.73 (s, 3F). LC/MS: 6.29 min retention time, 98.3% pure. ESI-MS 674 $[\text{M} + \text{H}]^+$. HRMS (ESI+) calcd for $\text{C}_{33}\text{H}_{38}\text{F}_3\text{N}_5\text{O}_7 + \text{H}$ 674.2802, found 674.2825.

ADME. The ADME experiments were performed at WuXi AppTech (Shanghai) using standard, validated protocols, and the results are the mean of experiments done in at least duplicate. Positive controls were used, and they performed within the acceptable range.

LogD was determined using a 100 mM phosphate buffer at pH 7.4 and 1-octanol using a shake flask method (shake 2 min and 1 h at a speed of 800 rpm at room temperature) and analysis by LC-MS/MS of the layers. The layers were diluted prior to analysis, and the LogD was equal to the log (mean octanol peak area ratio \times octanol dilution factor/mean buffer peak area ratio \times buffer layer dilution factor).

Plasma stability was performed using pooled frozen CD-1 mouse plasma that was thawed at 37 °C prior to experiment. Compounds were tested at 2 μM concentration at 37 °C (2% final DMSO concentration). The concentration of compound relative to the internal standard was determined at time points of 0, 10, 30, 60, and 120 min after acetonitrile precipitation. The analysis was performed by LC-MS/MS relative to an internal standard after centrifuging the sample.

Mouse (CD-1) Microsomal stability was performed at 37 °C with constant shaking. Incubation was done with and without the addition of NADPH with 0.5 mg protein/mL, compound concentration of 1 μM , control at 1 μM , DMSO 0.01%, and acetonitrile 0.99%. The compound concentration was determined by LC-MS/MS at 0, 5, 10, 20, 30, and 60 min.

Mouse (CD-1) hepatocyte stability was performed 37 °C with constant shaking in a 95% humidified incubator with 5% CO_2 . Incubation was done with and without hepatocytes with 0.5×10^6 cells/mL, compound concentration of 1 μM , positive compound at 3 μM , DMSO 0.01%, and acetonitrile 0.90%. The compound concentration was determined by LC-MS/MS at 0, 15, 30, 60, and 90 min.

Caco-2 cells purchased from ATCC were seeded onto polyethylene (PET) membranes in 96-well Corning Insert plates at 1×10^5 cells/cm 2 , and the medium was refreshed every 4 to 5 days until the 21st to 28th day for confluent cell monolayer formation. The transport buffer was at pH 7.4, and the compounds were tested at 2.0 μM bidirectionally (DMSO concentration <1%). The plate was incubated for 2 h in a CO_2 incubator at 37 °C with 5% CO_2 at saturated humidity without shaking. The samples were mixed with acetonitrile with an internal standard, and the quantities of the compounds were determined by LC-MS/MS in starting, donor, and receiver solutions. The Caco-2 monolayer integrity was determined after each assay.

pK_a Determination. Nonliterature pK_a values were determined by a pH titration of 20–40 mM solution of compound in a 20:1 mixture

of water/DMSO as reported by Albert and Serjeant.⁶⁰ The pH was measured with a Mettler Toledo SevenCompact pH/Ion S220 instrument that was calibrated with pH 1.00, 4.00, 7.00, and 10.00 standard buffers prior to each titration. The titrant (0.049 to 0.054 N NaOH) was delivered with a syringe pump at a 1 mL/min flow rate into the magnetically stirred solution. The carboxylic acids corresponding to compounds **15l**, **15m**, **15n**, and **15o** were converted into the hydrochloride salts prior to the titration to determine the pK_a of the carboxylic acid group.

Human Plasma Stability. A test compound (1 μ L of 5 mM DMSO solution) was incubated with human plasma (49 μ L, Sigma-Aldrich, P9523-5 ML) at 37 °C for a period of 15, 30, 60, and/or 120 min. The final concentration of the compound was 100 μ M with 2.0% DMSO. The incubation was terminated by the addition of 450 μ L of acetonitrile containing reserpine (5 μ M) as an internal standard. Following centrifugation at 15 000 rpm for 3 min, the concentration of the test compound along with the hydrolyzed product in the supernatant was quantified by LC/MS using the standard curve (Eluent E1 (isocratic 60% methanol–water for 6 min), Eluent E2 (isocratic 65% methanol–water for 6 min), or Eluent E3 (gradient of methanol–water, 65 to 85% in 2 min, followed by 4 min of isocratic methanol–water 85%)). The mean value of two independent experiments with two injections per sample is reported.

Human CatS Inhibition. The commercial CatS (CTSS, EC 3.4.22.27) inhibitor fluorometric assay kit (ab185437) from Abcam (UK) and the accompanying instructions and protocols were utilized. A 96-well white plate with a flat bottom and PerkinElmer's EnSpire multimode plate reader were used. Blank, enzyme, and inhibitor (supplied) controls were simultaneously tested for the inhibitors in triplicate. The test inhibitors were dissolved in and diluted in DMSO, and the DMSO final concentration was 1%. The compounds were screened at 1 μ M, and for IC_{50} determination, six different concentrations (4, 1, 0.25, 0.0625, 0.0156, and 0.0039 μ M) were tested. Protocols from Abcam were followed, with the exception that incubation was for 30 min at room temperature instead of 15 min. All test inhibitors and controls were run in triplicate for each concentration. The slope of enzyme control (EC) and the slope of test inhibitors (S) were calculated (linear regression), and the % relative inhibition was determined, as in the kit instructions. IC_{50} values were calculated using Prism 9 for Windows 64-bit (V 9.1.0) by GraphPad Software, and standard error is reported.

Human CatB Inhibition. The commercial Cathepsin B (CTSB, EC 3.4.22.1) inhibitor fluorometric assay kit (K147-100) from BioVision (USA) and the accompanying instructions and protocols were utilized. The test was performed identical to CatS, other than the final concentrations and the fact that the BioVision protocols followed a 30 min incubation period instead of 15 min. For **15h** and **15l**, the final concentrations of 4, 1, 0.25, 0.0625, 0.0156, and 0.0039 μ M were used, and for **15e**, 40, 10, 2.5, 0.625, 0.156, and 0.039 μ M were used. All concentrations were performed in triplicate.

■ ASSOCIATED CONTENT

SI Supporting Information

The Supporting Information is available free of charge at <https://pubs.acs.org/doi/10.1021/acs.jmedchem.1c00616>.

Glutathione stability studies (Table S1); protease, antiviral, and cytotoxicity graphs for **15l**; slopes of k_{obs} versus [I] for **15a**, **15e**, **15f**, **15h**, and **15l** (Table S2 and Charts S1 and S2); electron density for SARS-CoV-2 3CLP – **15l** active sites (Figure S1); SARS-CoV-2 3CLP – **15l** ligand plot (Figure S2) and crystallographic data (Table S3); and ¹H NMR, ¹⁹F NMR, and HPLC for select compounds (PDF)

Molecular formula strings for all compounds with biological data (CSV)

■ AUTHOR INFORMATION

Corresponding Author

James A. Nieman – Li Ka Shing Applied Virology Institute and Department of Medical Microbiology and Immunology, University of Alberta, Edmonton, Alberta T6G 2E1, Canada; orcid.org/0000-0002-5087-0819; Phone: +1-(780) 492-8704; Email: jnieman@ualberta.ca

Authors

Bing Bai – Li Ka Shing Applied Virology Institute and Department of Medical Microbiology and Immunology, University of Alberta, Edmonton, Alberta T6G 2E1, Canada

Alexandr Belovodskiy – Li Ka Shing Applied Virology Institute and Department of Medical Microbiology and Immunology, University of Alberta, Edmonton, Alberta T6G 2E1, Canada

Mostofa Hena – Li Ka Shing Applied Virology Institute and Department of Medical Microbiology and Immunology, University of Alberta, Edmonton, Alberta T6G 2E1, Canada

Appan Srinivas Kandadai – Li Ka Shing Applied Virology Institute and Department of Medical Microbiology and Immunology, University of Alberta, Edmonton, Alberta T6G 2E1, Canada

Michael A. Joyce – Li Ka Shing Institute of Virology and Department of Medical Microbiology and Immunology, University of Alberta, Edmonton, Alberta T6G 2E1, Canada

Holly A. Saffran – Li Ka Shing Institute of Virology and Department of Medical Microbiology and Immunology, University of Alberta, Edmonton, Alberta T6G 2E1, Canada

Justin A. Shields – Li Ka Shing Institute of Virology and Department of Medical Microbiology and Immunology, University of Alberta, Edmonton, Alberta T6G 2E1, Canada

Muhammad Bashir Khan – Department of Biochemistry, University of Alberta, Edmonton, Alberta T6G 2H7, Canada

Elena Arutyunova – Li Ka Shing Institute of Virology, University of Alberta, Edmonton, Alberta T6G 2E1, Canada; Department of Biochemistry, University of Alberta, Edmonton, Alberta T6G 2H7, Canada

Jimmy Lu – Li Ka Shing Institute of Virology, University of Alberta, Edmonton, Alberta T6G 2E1, Canada; Department of Biochemistry, University of Alberta, Edmonton, Alberta T6G 2H7, Canada

Sardeep K. Bajwa – Department of Biochemistry, University of Alberta, Edmonton, Alberta T6G 2H7, Canada

Darren Hockman – Li Ka Shing Applied Virology Institute and Department of Medical Microbiology and Immunology, University of Alberta, Edmonton, Alberta T6G 2E1, Canada

Conrad Fischer – Department of Chemistry, University of Alberta, Edmonton, Alberta T6G 2G2, Canada; Present Address: Department of Physical Sciences, Barry University, 11300 NE Second Avenue, Miami Shores, Florida 33161, United States

Tess Lamer – Department of Chemistry, University of Alberta, Edmonton, Alberta T6G 2G2, Canada

Wayne Vuong – Department of Chemistry, University of Alberta, Edmonton, Alberta T6G 2G2, Canada; orcid.org/0000-0002-3439-8788

Marco J. van Belkum – Department of Chemistry, University of Alberta, Edmonton, Alberta T6G 2G2, Canada

Zhengxian Gu – WuXi AppTec (Shanghai) Co., Ltd., Shanghai 200131, China

Fusen Lin – WuXi AppTec (Shanghai) Co., Ltd., Shanghai 200131, China

Yanhua Du – WuXi AppTec (Shanghai) Co., Ltd., Shanghai 200131, China

Jia Xu – WuXi AppTec (Shanghai) Co., Ltd., Shanghai 200131, China

Mohammad Rahim – Rane Pharmaceuticals, Inc., Edmonton, Alberta T6E 5V2, Canada

Howard S. Young – Department of Biochemistry, University of Alberta, Edmonton, Alberta T6G 2H7, Canada

John C. Vederas – Department of Chemistry, University of Alberta, Edmonton, Alberta T6G 2G2, Canada;

orcid.org/0000-0002-2996-0326

D. Lorne Tyrrell – Li Ka Shing Applied Virology Institute, Li Ka Shing Institute of Virology, and Department of Medical Microbiology and Immunology, University of Alberta, Edmonton, Alberta T6G 2E1, Canada

M. Joanne Lemieux – Li Ka Shing Institute of Virology, University of Alberta, Edmonton, Alberta T6G 2E1, Canada; Department of Biochemistry, University of Alberta, Edmonton, Alberta T6G 2H7, Canada; orcid.org/0000-0003-4745-9153

Complete contact information is available at:

<https://pubs.acs.org/10.1021/acs.jmedchem.1c00616>

Funding

Funding for the project was provided by Alberta Innovates (RES27408) and the Canadian Institutes of Health Research Rapid Research (VR3-172655).

Notes

The authors declare no competing financial interest.

ACKNOWLEDGMENTS

We thank numerous colleagues at the University of Alberta including Vishwa Somayaji (Faculty of Pharmacy and Pharmaceutical Sciences) for running ^1H , ^{13}C , and ^{19}F NMR; Jack Moore (Alberta Proteomics and Mass Spectrometry Facility) for HMRS; and the Analytical and Instrumentation Laboratory (Department of Chemistry) for performing the elemental analyses. We also thank the DMPK group at WuXi AppTech for performing the ADME experiments reported in Table 3. We thank the staff at SSRL beamline 12-1, in particular Dr. Silvia Russi. Use of the Stanford Synchrotron Radiation Lightsource, SLAC National Accelerator Laboratory, is supported by the U.S. Department of Energy, Office of Science, Office of Basic Energy Sciences under Contract No. DE-AC02-76SF00515. The SSRL Structural Molecular Biology Program is supported by the DOE Office of Biological and Environmental Research, and by the National Institutes of Health, National Institute of General Medical Sciences (P30GM133894). The contents of this publication are solely the responsibility of the authors and do not necessarily represent the official views of NIGMS or NIH.

ABBREVIATIONS USED

3CLP, 3-chymotrypsin-like protease; 3CP, 3-C protease; ADME, absorption, distribution, metabolism, and excretion; AMK, α -acyloxymethylketone; Boc, *tert*-butyloxycarbonyl; CoV, coronavirus; COVID-19, coronavirus disease 2019; CPE, cytopathic effect; DCM, dichloromethane; DMF, *N,N*-dimethylformamide; DMSO, dimethyl sulfoxide; EtOAc, ethyl acetate; Et₃N, triethylamine; FIP, feline infectious peritonitis; HATU, 1-[bis(dimethylamino) methylene]-1*H*-1,2,3-triazolo[4,5-*b*]pyridinium 3-oxide hexafluorophosphate; MeOH,

methanol; NMM, *N*-methylmorpholine; PK, pharmacokinetic; PRA, plaque reduction assay; SARS, severe acute respiratory syndrome; SI, selectivity index; *t*Bu, *tert*-butyl; THF, tetrahydrofuran

REFERENCES

- (1) (a) Baltimore, D. Expression of Animal Virus Genomes. *Bacteriol. Rev.* **1971**, *35*, 235–241. (b) Berman, J. J. Group IV Viruses: Single-Stranded (+)Sense RNA. *Taxonomic Guide to Infectious Diseases* **2012**, 237–246.
- (2) Dragovich, P. S.; Prins, T. J.; Zhou, R.; Webber, S. E.; Marakovits, J. T.; Fuhrman, S. A.; Patick, A. K.; Matthews, D. A.; Lee, C. A.; Ford, C. E.; Burke, B. J.; Rejto, R. A.; Hendrickson, T. F.; Tuntland, T.; Brown, E. L.; Meador, J. W., III; Ferre, R. A.; Harr, J. E. V.; Kosa, M. B.; Worland, S. T. Structure-Based Design, Synthesis, and Biological Evaluation of Irreversible Human Rhinovirus 3C Protease Inhibitors. 4. Incorporation of P1 Lactam Moieties as L-Glutamine Replacements. *J. Med. Chem.* **1999**, *42*, 1213–1224.
- (3) Center for Disease Control and Prevention. <https://www.cdc.gov/norovirus/trends-outbreaks/worldwide.html> (accessed 2021-02-06).
- (4) Gil, C.; Ginex, T.; Maestro, I.; Nozal, V.; Barrado-Gil, L.; Cuesta-Geijo, M.Á.; Urquiza, J.; Ramírez, D.; Alonso, C.; Campillo, N. E.; Martínez, A. COVID-19: Drug Targets and Potential Treatments. *J. Med. Chem.* **2020**, *63*, 12359–12386.
- (5) Lau, S.K. P.; Lee, P.; Tsang, A.K. L.; Yip, C.C. Y.; Tse, H.; Lee, R. A.; So, L.-Y.; Lau, Y.-L.; Chan, K.-H.; Woo, P. C. Y.; Yuen, K.-Y. Molecular Epidemiology of Human Coronavirus OC43 Reveals Evolution of Different Genotypes over Time and Recent Emergence of a Novel Genotype due to Natural Recombination. *J. Virol.* **2011**, *85* (21), 11325–11337.
- (6) Centers for Disease Control and Prevention. <https://www.cdc.gov/coronavirus/types.html> (accessed 2021-02-06).
- (7) Anirudhan, V.; Lee, H.; Cheng, H.; Cooper, L.; Rong, L. Targeting SARS-CoV-2 Viral Proteases as a Therapeutic Strategy to Treat COVID-19. *J. Med. Virol.* **2021**, *93*, 2722–2734.
- (8) (a) Long, A. C.; Orr, D. C.; Cameron, J. M.; Dunn, B. M.; Kay, J. A consensus sequence for substrate hydrolysis by rhinovirus 3C proteinase. *FEBS Lett.* **1989**, *258* (1), 75–78. (b) May, J.; Viswanathan, P.; Ng, K.K.-S.; Medvedev, A.; Korba, B. The P4-P2' Amino Acids Surrounding Human Norovirus Polyprotein Cleavage Sites Define the Core Sequence Regulating Self-Processing Order. *J. Virol.* **2014**, *88* (18), 10738–10747. (c) Xiong, M.; Su, H.; Zhao, W.; Xie, H.; Shao, Q.; Xu, Y. What coronavirus 3C-like protease tells us: From structure, substrate selectivity, to inhibitor design. *Med. Res. Rev.* **2021**, *41* (4), 1965–1998. (d) Zhang, L.; Lin, D.; Kusov, Y.; Nian, Y.; Ma, Q.; Wang, J.; von Brunn, A.; Leyssen, P.; Lanko, K.; Neyts, J.; de Wilde, A.; Snijder, E. J.; Liu, H.; Hilgenfeld, R. α -Ketoamides as broad-spectrum inhibitors of coronavirus and enterovirus replication: structure-based design, synthesis, and activity assessment. *J. Med. Chem.* **2020**, *63* (9), 4562–4578.
- (9) Hayden, F. G.; Turner, R. B.; Gwaltney, J. M.; Chi-Burris, K.; Gersten, M.; Hsyu, P.; Patick, A. K.; Smith, G. J., III; Zalman, L. S. Randomized, Double-Blind, Placebo-Controlled Studies of Rupintrivir Nasal Spray 2-Percent Suspension for Prevention and Treatment of Experimentally Induced Rhinovirus Colds in Healthy Volunteers. *Antimicrob. Agents Chemother.* **2003**, *47* (12), 3907–3916.
- (10) Galasiti Kankanamalage, A. C.; Kim, Y.; Weerawarna, P. M.; Uy, R. A. Z.; Damalanka, V. C.; Mandadapu, S. R.; Alliston, K. R.; Mehzebene, N.; Battaile, K. P.; Lovell, S.; Chang, K.-O.; Groutas, W. C. Structure-Guided Design and Optimization of Dipeptidyl Inhibitors of Norovirus 3CL Protease. Structure–Activity Relationships and Biochemical, X-ray Crystallographic, Cell-Based, and *In Vivo* Studies. *J. Med. Chem.* **2015**, *58*, 3144–3155.
- (11) Hoffman, R. L.; Kania, R. S.; Nieman, J. A.; Planken, S. P.; Smith, G. J. Anticoronaviral Compounds and Compositions, Their Pharmaceutical Uses and Materials For Their Synthesis. WO2005/113580, May 9, 2005.

- (12) Freedman, H.; Kundu, J.; Tchesnokov, P. E.; Law, J. L. M.; Nieman, J. A.; Schinazi, R. F.; Tyrrell, D. L.; Gotte, M.; Houghton, M. Application of Molecular Dynamics Simulations to the Design of Nucleotide Inhibitors Binding to Norovirus Polymerase. *J. Chem. Inf. Model.* **2020**, *60*, 6566–6578.
- (13) Rathnayake, A. D.; Kim, Y.; Dampalla, C. S.; Nguyen, H. N.; Jesri, A.-R. M.; Kashipathy, M. M.; Lushington, G. H.; Battaile, K. P.; Lovell, S.; Chang, K.-O.; Groutas, W. C. Structure-Guided Optimization of Dipeptidyl Inhibitors of Norovirus 3CL Protease. *J. Med. Chem.* **2020**, *63* (20), 11945–11963.
- (14) World Health Organization. <http://www.who.int/emergencies/diseases/novel-coronavirus-2019> (accessed 2021-02-06).
- (15) Pardo, J.; Shukla, A. M.; Chamarthi, G.; Gupta, A. The journey of remdesivir: from Ebola to COVID-19. *Drugs in Context* **2020**, *9*, 1–9.
- (16) U.S. Food and Drug Administration. <https://www.fda.gov/news-events/press-announcements/fda-approves-first-treatment-covid-19> (accessed 2021-02-06).
- (17) Sheahan, T. P.; Sims, A. C.; Zhou, S.; Graham, R. L.; Pruijssers, A. J.; Agostini, M. L.; Leist, S. R.; Schafer, A.; Dinno, K. H.; Stevens, L. J.; Chappell, J. D.; Lu, X.; Hughes, T. M.; George, A. S.; Hill, C. S.; Montgomery, S. A.; Brown, A. J.; Bluemling, G. R.; Natchus, M. G.; Saindane, M.; Kolykhalov, A. A.; Painter, G.; Harcourt, J.; Tamin, A.; Thornburg, N. J.; Swanstrom, R.; Denison, M. R.; Baric, R. S. An orally bioavailable broad-spectrum antiviral inhibits SARS-CoV-2 in human airway epithelial cell cultures and multiple coronaviruses in mice. *Sci. Transl. Med.* **2020**, *12*, eabb5883.
- (18) (a) Turk, B. Targeting proteases: success, failures and future prospects. *Nat. Rev. Drug Discovery* **2006**, *5*, 785–799. (b) Hamada, Y.; Kiso, Y. New Directions for Protease Inhibitors Directed Drug Discovery. *Biopolymers* **2016**, *106*, 563–579.
- (19) McClung, M. R.; O'Donoghue, M. L.; Papapoulos, S. E.; Bone, H.; Langdahl, B.; Saag, K. G.; Reid, I. R.; Kiel, D. P.; Cavallari, L.; Marc, P.; Bonaca, M. P.; Wiviott, S. D.; de Villiers, T.; Ling, X.; Lippuner, K.; Nakamura, T.; Reginster, J.-Y.; Rodriguez-Portales, J. A.; Roux, C.; Zanchetta, J.; Zerbin, C. A. F.; Park, J.-G.; Im, K.; Cange, A.; Grip, L. T.; Heyden, N.; DaSilva, C.; Cohn, D.; Massaad, R.; Scott, B. B.; Verbruggen, N.; Gurner, D.; Miller, D. L.; Blair, M. L.; Polis, A. B.; Stoch, S. A.; Santora, A.; Lombardi, A.; Leung, A. T.; Kaufman, K. D.; Marc, S.; Sabatine, M. S.; et al. Olanacatib for the treatment of postmenopausal osteoporosis: results of the LOFT multicentre, randomised, double-blind, placebo-controlled trial and LOFT Extension study. *Lancet Diabetes Endocrinol.* **2019**, *7* (12), 899–911.
- (20) Singh, J.; Petter, R. C.; Baillie, T. A.; Whitty, A. The resurgence of covalent drugs. *Nat. Rev. Drug Discovery* **2011**, *10*, 307–317.
- (21) Ghosh, A. K.; Samanta, I.; Mondal, A.; Liu, W. R. Covalent Inhibition in Drug Discovery. *ChemMedChem* **2019**, *14* (9), 889–906.
- (22) Halford, B. Covalent drugs go from fringe field to fashionable endeavor. *C&EN* **2020**, *98* (43), 28–33.
- (23) Gallwitz, B. Clinical Use of DPP-4 Inhibitors. *Front. Endocrinol.* **2019**, *10*, 389.
- (24) Forman, H. J.; Zhang, H.; Rinna, A. Glutathione: Overview of its protective roles, measurement, and biosynthesis. *Mol. Aspects Med.* **2009**, *30* (1–2), 1–12.
- (25) Reviews of repurposed and targeted peptidomimetics: Citarella, A.; Scala, A.; Piperno, A.; Micale, N. SARS-CoV-2 Mpro: A Potential Target for Peptidomimetics and Small-Molecule Inhibitors. *Biomolecules* **2021**, *11* (11), 607. Cui, W.; Yang, K.; Yang, H. Yang K and Yang H Recent Progress in the Drug Development Targeting SARS-CoV-2 Main Protease as Treatment for COVID-19. *Front. Mol. Biosci.* **2020**, *7*, 616341. Cannalire, R.; Cerchia, C.; Beccari, A. R.; Di Leva, F. S.; Summa, V. Targeting SARS-CoV-2 Proteases and Polymerase for COVID-19 Treatment: State of the Art and Future Opportunities. *J. Med. Chem.* **2021**, DOI: 10.1021/acs.jmedchem.0c01140.
- (26) Pillaiyar, T.; Manickam, M.; Namasivayam, V.; Hayashi, Y.; Jung, S.-H. An Overview of Severe Acute Respiratory Syndrome–Coronavirus (SARS-CoV) 3CL Protease Inhibitors: Peptidomimetics and Small Molecule Chemotherapy. *J. Med. Chem.* **2016**, *59*, 6595–6628.
- (27) Dai, W.; Zhang, B.; Jiang, X.-M.; Su, H.; Li, J.; Zhao, Y.; Xie, X.; Jin, Z.; Peng, J.; Liu, F.; Li, C.; Li, Y.; Bai, F.; Wang, H.; Cheng, X.; Cen, X.; Hu, S.; Yang, X.; Wang, J.; Liu, X.; Xiao, G.; Jiang, H.; Rao, Z.; Zhang, L.-K.; Xu, Y.; Yang, H.; Liu, H. Structure-based design of antiviral drug candidates targeting the SARS-CoV-2 main protease. *Science* **2020**, *368*, 1331–1335.
- (28) Qiao, J.; Li, Y.-S.; Zeng, R.; Liu, F.-L.; Luo, R.-H.; Huang, C.; Wang, Y.-F.; Zhang, J.; Quan, B.; Shen, C.; Mao, X.; Liu, X.; Sun, W.; Yang, W.; Ni, X.; Wang, K.; Xu, L.; Duan, Z.-L.; Zou, Q.-C.; Zhang, H.-L.; Qu, W.; Long, Y.-H.-P.; Li, M.-H.; Yang, R.-C.; Liu, X.; You, J.; Zhou, Y.; Yao, R.; Li, W.-P.; Liu, J.-M.; Chen, P.; Liu, Y.; Lin, G.-F.; Yang, X.; Zou, J.; Li, L.; Hu, Y.; Lu, G.-W.; Li, W.-M.; Wei, Y.-Q.; Zheng, Y.-T.; Lei, J.; Yang, S. SARS-CoV-2 Mpro inhibitors with antiviral activity in a transgenic mouse model. *Science* **2021**, *371*, 1374–1378.
- (29) Zhang, L.; Lin, D.; Sun, X.; Curth, U.; Drosten, C.; Sauerhering, L.; Becker, S.; Rox, K.; Hilgenfeld, R. Crystal structure of SARS-CoV-2 main protease provides a basis for design of improved α -ketoamide inhibitors. *Science* **2020**, *368*, 409–412.
- (30) Jin, Z.; Du, X.; Xu, Y.; Deng, Y.; Liu, L.; Zhao, Y.; Zhang, B.; Li, X.; Zhang, L.; Peng, C.; Duan, Y.; Yu, J.; Wang, L.; Yang, K.; Liu, F.; Jiang, R.; Yang, X.; You, T.; Liu, X.; Yang, X.; Bai, F.; Liu, H.; Liu, X.; Guddat, L. W.; Xu, W.; Xiao, G.; Qin, C.; Shi, Z.; Jiang, H.; Rao, Z.; Yang, H. Structure of Mpro from SARS-CoV-2 and discovery of its inhibitors. *Nature* **2020**, *582*, 289–293.
- (31) (a) Smith, R. A.; Copp, L. J.; Coles, P. J.; Pauls, H. W.; Robinson, V. J.; Spencer, R. W.; Heard, S. B.; Krantz, A. New Inhibitors of Cysteine Proteinases. Peptidyl Acyloxymethylketones and the Quiescent Nucleofuge Strategy. *J. Am. Chem. Soc.* **1988**, *110*, 4429–4431. (b) Krantz, A.; Copp, L. J.; Coles, P. J.; Smith, R. A.; Heard, S. B. Peptidyl (Acyloxy)methyl Ketones and the Quiescent Affinity Label Concept: The Departing Group as a Variable Structure Element in the Design of Inactivators of Cysteine Proteinases. *Biochemistry* **1991**, *30*, 4678–4687. (c) Robinson, V. J.; Pauls, H. W.; Coles, P. J.; Smith, R. A.; Krantz, A. Carbon-13 NMR characterization of the Papain Adduct Formed by Peptidyl Acyloxy-, Aryloxy, and Chloromethyl Ketone Irreversible Inhibitors. *Bioorg. Chem.* **1992**, *20*, 42–54.
- (32) Yeo, E. H.; Goh, W. L.; Chow, S. C. The aminopeptidase inhibitor, z-CMK, is toxic and induces cell death in Jurkat T cells through oxidative stress. *Toxicol. Mech. Methods* **2018**, *28* (3), 157–166.
- (33) Eichhold, T. H.; Hookfin, E. B.; Taiwo, Y. O.; De, B.; Wehmeyer, K. R. Isolation and quantification of fluoroacetate in rat tissues, following dosing of Z-Phe-Ala-CH₂-F, a peptidyl fluoromethyl ketone protease inhibitor. *J. Pharm. Biomed. Anal.* **1997**, *16* (3), 459–467.
- (34) Dolle, R. E.; Singh, J.; Whipple, D.; Osifo, I. K.; Speier, G.; Graybill, T. L.; Gregory, J. S.; Harris, A. L.; Helaszek, C. T. Aspartyl α -((Diphenylphosphinyl)oxy) methyl Ketones as Novel Inhibitors of Interleukin-1 β Converting Enzyme. Utility of the Diphenylphosphinic Acid Leaving Group for the Inhibition of Cysteine Proteinases. *J. Med. Chem.* **1995**, *38* (38), 220–222. Graybill, T. L.; Prouty, C. P.; Speier, G. J.; Hoyer, D.; Dolle, R. E.; Helaszek, C. T.; Ator, M. A.; Uhl, J.; Strastes, J. α -((Tetronoyl)oxy)- and α -((Tetramoyl)oxy)-methyl ketone inhibitors of the interleukin-1 β converting enzyme (ICE). *Bioorg. Med. Chem. Lett.* **1997**, *7* (1), 41–46.
- (35) Dai, Y.; Hedstrom, L.; Abeles, R. H. Inactivation of Cysteine Proteinases by (Acyloxy)methyl Ketones Using S'-P' Interactions. *Biochemistry* **2000**, *39*, 6498–6502.
- (36) van de Plassche, M. A. T.; Barniol-Xicota, M.; Verhelst, S. H. L. Peptidyl Acyloxymethyl Ketones as Activity-Based Probes for the Main Protease of SARS-CoV-2. *ChemBioChem* **2020**, *21*, 3383–3388.
- (37) Liu, Y.; Liang, C.; Xin, L.; Ren, X.; Tian, L.; Ju, X.; Li, H.; Wang, Y.; Zhao, Q.; Liu, H.; Cao, W.; Xie, X.; Zhang, D.; Wang, Y.; Jian, Y. The development of Coronavirus 3C-Like protease (3CLpro) inhibitors from 2010 to 2020. *Eur. J. Med. Chem.* **2020**, *206*, 112711.
- (38) Zhai, Y.; Zhao, X.; Cui, Z.; Wang, M.; Wang, Y.; Li, L.; Sun, Q.; Yang, X.; Zeng, D.; Liu, Y.; Sun, Y.; Lou, Z.; Shang, L.; Yin, Z.

Cyanohydrin as an Anchoring Group for Potent and Selective Inhibitors of Enterovirus 71 3C Protease. *J. Med. Chem.* **2015**, *58*, 9414–9420.

(39) Hoffman, R. L.; Kania, R. S.; Brothers, M. A.; Davies, F. F.; Ferre, R. A.; Gajiwala, K. S.; He, M.; Hogan, R. J.; Kozminski, K.; Li, L. Y.; Lockner, J. W.; Lou, J.; Marra, M. T.; Mitchell, L. J., Jr.; Murray, B. W.; Nieman, J. A.; Noell, S.; Planken, S. P.; Rowe, T.; Ryan, K.; Smith, G. J., III; Solowiej, J. E.; Stepan, C. M.; Taggart, B. Discovery of Ketone-Based Covalent Inhibitors of Coronavirus 3CL Proteases for the Potential Therapeutic Treatment of COVID-19. *J. Med. Chem.* **2020**, *63*, 12725–12747.

(40) Halford, B. Pfizer's novel COVID-19 antiviral heads to clinical trials. *C&EN* **2020**, *98* (37), 9.

(41) Ieda, S.; Kan, T.; Fukuyama, T. Synthesis of the optically active key intermediate of FR901483. *Tetrahedron Lett.* **2010**, *51*, 4027–4029.

(42) Vuong, W.; Khan, M. B.; Fischer, C.; Arutyunova, E.; Lamer, T.; Shields, J.; Saffran, H. A.; McKay, R. T.; van Belkum, M. J.; Joyce, M. A.; Young, H. S.; Tyrrell, D. L.; Vederas, J. C.; Lemieux, M. J. Feline coronavirus drug inhibits the main protease of SARS-CoV-2 and blocks virus replication. *Nat. Commun.* **2020**, *11* (1), 4282.

(43) Thorarensen, A.; Balbo, P.; Banker, M. E.; Czerwinski, R. M.; Kuhn, M.; Maurer, T. S.; Telliez, J.-B.; Vincent, F.; Wittwer, A. J. The advantages of describing covalent inhibitor in vitro potencies by IC₅₀ at a fixed time point: IC₅₀ determination of covalent inhibitors provides meaningful data to medicinal chemistry for SAR optimization. *Bioorg. Med. Chem.* **2021**, *29*, 115865.

(44) (a) Vuong, W.; Fischer, C.; Khan, M. B.; van Belkum, M. J.; Lamer, T.; Willoughby, K. D.; Lu, J.; Arutyunova, E.; Joyce, M. A.; Saffran, H. A.; Shields, J. A.; Young, H. S.; Nieman, J. A.; Tyrrell, D. L.; Lemieux, M. J.; Vederas, J. C. Improved SARS-CoV-2 Mpro inhibitors based on feline coronavirus drug GC376: structure-activity studies and solubilization for enhanced bioavailability. *Eur. J. Med. Chem.* **2021**, *222*, 113584. (b) Arutyunova, E.; Khan, M. B.; Fischer, C.; Lu, J.; Lamer, T.; Vuong, W.; van Belkum, M. J.; McKay, R. T.; Tyrrell, D. L.; Vederas, J. C.; Young, H. S.; Lemieux, M. J. N-Terminal finger stabilizes the S1 Pocket for the reversible feline drug GC376 in SARS-CoV-2 M^{pro} Dimer. *J. Mol. Biol.* **2021**, *433* (13), 167003.

(45) Ma, C.; Sacco, M. D.; Hurst, B.; Townsend, J. A.; Hu, Y.; Szeto, T.; Zhang, X.; Tarbet, B.; Marty, M. T.; Chen, Y.; Wang, J. Boceprevir, GC-376, and calpain inhibitors II, XII inhibit SARS-CoV-2 viral replication by targeting the viral main protease. *Cell Res.* **2020**, *30*, 678–692.

(46) Mengist, H. M.; Mekonnen, D.; Mohammed, A.; Shi, R.; Jin, T. Potency, Safety, and Pharmacokinetic Profiles of Potential Inhibitors Targeting SARS-CoV-2 Main Protease. *Front. Pharmacol.* **2021**, *11*, 630500.

(47) (a) Liu, X.; Testa, B.; Fahr, A. Lipophilicity and Its Relationship with Passive Drug Permeation. *Pharm. Res.* **2011**, *28*, 962–977. (b) Yang, N. J.; Hinner, M. J. Getting Across the Cell Membrane: An Overview for Small Molecules, Peptides, and Proteins. *Methods Mol. Biol.* **2015**, *1266*, 29–53.

(48) (a) Yukawa, T.; Naven, R. Utility of Physicochemical Properties for the Prediction of Toxicological Outcomes: Takeda Perspective. *ACS Med. Chem. Lett.* **2020**, *11* (2), 203–209. (b) Kiani, Y. S.; Jabeen, I. Lipophilic Metabolic Efficiency (LipMetE) and Drug Efficiency Indices to Explore the Metabolic Properties of the Substrates of Selected Cytochrome P450 Isoforms. *ACS Omega* **2020**, *5*, 179–188. (c) Tinworth, C. P.; Young, R. J. Facts, Patterns and Principles in Drug Discovery: Appraising the Rule of 5 with Measured Physicochemical Data. *J. Med. Chem.* **2020**, *63*, 10091–10108. (d) Caron, G.; Kihlberg, J.; Goetz, G.; Ratkova, E.; Poongavanam, V.; Ermondi, G. Steering New Drug Discovery Campaigns: Permeability, Solubility and Physicochemical Properties in the bRo5 Chemical Space. *ACS Med. Chem. Lett.* **2021**, *12*, 13–23.

(49) Dissociation Constants of Organic Acids and Bases. In *CRC Handbook of Chemistry and Physics*, 88th ed.; Lide, D. R., Ed.; CRC Press, 2007; pp 8-42–8-51.

(50) Dhareshwar, S. S.; Stella, V. J. Chapter 3.2. Prodrugs of Alcohols and Phenols. In *Prodrugs: Challenges and Rewards Part 1*; Stella, V. J., Borchardt, R. T., Hageman, M. J., Oliyai, R., Maag, H., Tilley, J. W., Eds.; Biotechnology: Pharmaceutical Aspects V; Springer: New York, 2007; pp 31–99.

(51) Biniossek, M. L.; Nägler, D. K.; Becker-Pauly, C.; Schilling, O. Proteomic Identification of Protease Cleavage Sites Characterizes Prime and Non-prime Specificity of Cysteine Cathepsin B L and S. *J. Proteome Res.* **2011**, *10*, 5363–5373.

(52) Brown, R.; Nath, S.; Lora, A.; Samaha, G.; Elgamal, Z.; Kaiser, R.; Taggart, C.; Weldon, S.; Geraghty, R. Cathepsin S: Investigating an old player in lung disease pathogenesis, comorbidities, and potential therapeutics. *Respir. Res.* **2020**, *21*, 111.

(53) Wang, H.; He, S.; Deng, W.; Zhang, Y.; Li, G.; Sun, J.; Zhao, W.; Guo, Y.; Yin, Z.; Li, D.; Shang, L. Comprehensive Insights into the Catalytic Mechanism of Middle East Respiratory Syndrome 3C-Like Protease and Severe Acute Respiratory Syndrome 3C-Like Protease. *ACS Catal.* **2020**, *10*, 5871–5890.

(54) Liu, H.; Jiang, S.; Dai, W.; Lu, L.; Peng, J.; Xia, S.; Wang, J.; Li, J.; Jiang, J.; Chen, K. Ketoamide Compound and Preparation Method, Pharmaceutical Composition and Use Thereof. WO2020/030143, September 8, 2019.

(55) McPhillips, T. M.; McPhillips, S. E.; Chiu, H. J.; Cohen, A. E.; Deacon, A. M.; Ellis, P. J.; Garman, E.; Gonzalez, A.; Sauter, N. K.; Phizackerley, R. P.; Soltis, S. M.; Kuhn, P. Blu-Ice and the Distributed Control System: software for data acquisition and instrument control at macromolecular crystallography beamlines. *J. Synchrotron Radiat.* **2002**, *9*, 401–406.

(56) Gonzalez, A.; Moorhead, P.; McPhillips, S. E.; Song, J.; Sharp, K.; Taylor, J. R.; Adams, P. D.; Sauter, N. K.; Soltis, S. M. Web-Ice: Integrated Data Collection and Analysis for Macromolecular Crystallography. *J. Appl. Crystallogr.* **2008**, *41*, 176–184.

(57) Wardrop, D. J.; Velter, A. I.; Forslund, R. E. Template-Directed C–H Insertion: Synthesis of the Dioxabicyclo[3.2.1]octane Core of the Zearagozic Acids. *Org. Lett.* **2001**, *3* (15), 2261–2264.

(58) Katsuyama, I.; Ogawa, S.; Yamaguchi, Y.; Funabiki, K.; Matsui, M.; Muramatsu, H.; Shibata, K. A Convenient and Regioselective Synthesis of 4-Trifluoromethylpyridines. *Synthesis* **1997**, *1997*, 1321–1324.

(59) Shibuya, K.; Tadaaki, O.; Toru, M. Method for Producing Cyclic Diamine Derivative or Salt Thereof. WO2004/106323 (EP1627875), May 28, 2003.

(60) Albert, A., Serjeant, E. P. *The Determination of Ionization Constants. A Laboratory Manual*, 3rd ed.; Chapman and Hall: New York, 1984.